

1 **Non-Invasive Measurement of Oil-Water Two-Phase Flow in Vertical Pipe Using**
2 **Ultrasonic Doppler Sensor and Gamma Ray Densitometer**

3

Baba Musa Abbagoni^{*,1,2} Hoi Yeung¹ and Lao Liyun¹

¹Energy and Power, Cranfield University, MK43 0AL, United Kingdom

²Department of Electrical and Electronic Engineering, University of Maiduguri,
PMB 1070, Bama Road, Maiduguri, Nigeria

***Corresponding author. E-mail address: bamusa08@gmail.com**

4

5

6

7

8

9 **Abstract**

10 Oil–water two-phase flow experiments were conducted in a vertical pipe to study the
11 liquid-liquid flow measurement using a non-invasive ultrasound Doppler flow sensor
12 and a gamma densitometer. Tap water and a dyed mineral oil are used as test the fluids.
13 A novel Doppler effect strategy is used to estimate the mixture flow velocity in a
14 vertical pipe based on flow velocity measured by the ultrasound sensor and the shear
15 flow velocity profile model. Drift-flux flow model was used in conjunction phase
16 fractions to predict the superficial velocities of oil and water. The results indicate that
17 the proposed method estimated oil-continuous flow and water-continuous flow have
18 average relative errors of 5.2% % and 4.5%; and superficial phase flow velocities of oil
19 and of water have average relative errors of 4.5% and 5.9% respectively. These results
20 demonstrate the potential for using ultrasonic Doppler sensor combined with gamma
21 densitometer for oil-water measurement.

22 **Keywords:**

23 liquid-liquid flow; drift-flux model; velocity profile; water fraction, phase superficial
24 velocity

25 **1 Introduction**

26 Oil-water two-phase flow is frequently encountered in the petroleum industry, for
27 example, in transportation pipelines between production wells and offshore platform
28 separators (Eskin et al., 2017). Accurate measurement of the oil-water two-phase flow
29 is very important and challenging for a range of applications, particularly for reservoir
30 assessment and management (Du et al., 2012), liquid production prediction and
31 control (Shi et al., 2017), produced water estimation and management (Zhai et al., 2013).
32 Importantly, as a oil field matures, the amount of water that would be produced together
33 with the oil in the well increases significantly (Hasan and Kabir, 1998; Lucas and Jin,
34 2001). The high water-cut oil-water flow causes a serious challenge to most multiphase
35 flow measurement instruments such as the device has to deal with are the influences of
36 small density difference between oil and water, flow regime and kinematic viscosity.
37 The differences in flow regimes is created by the Kinematic viscosity (Dong et al.,
38 2015).

39 Several attempts at measuring oil-water two-phase flow in both horizontal and vertical
40 pipe using either a single or multiple instruments were successful (Shamsul et al.,
41 2015). Single sensing device is often use in measuring a parameter of flow such as
42 velocity, phase volume fraction, pressure gradient, flow pattern identification and
43 characterisation (Shamsul et al., 2015). For example, sensors frequently used in
44 measuring oil-water flow include pressure transducers (Da et al., 2007; Flores et al.,
45 1998; Shamsul et al., 2015), ultrasonic sensors (Dong et al., 2015; Kouame et al., 2003;
46 Morriss and Hill, 1991; Tan et al., 2016), gamma densitometer (Descamps et al., 2006;
47 Kumara et al., 2010a; Tesi, 2011), conductance probes (Chen et al., 2015; Du et al.,

48 2012; Jana et al., 2006; Oddie, 1992; Shamsul et al., 2015) capacitance probes(Ismail et
49 al., 2005) and electromagnetic flowmeters(Faraj et al., 2015; Jin et al., 2020).

50 As a matter of fact, a comprehensive measurement of two-phase flow requires use of at
51 least two different devices or two independent outputs of one device. Experimental
52 studies on measurement of oil–water flow using two-sensor methods are plenty. For
53 example, Conductance Ring Coupled Cone (CRCC) meter (Tan et al., 2015),
54 electromagnetic flowmeter(EMFM) and electrical resistance tomography (ERT)(Faraj et
55 al., 2015), EMFM combined with a plug-in conductance sensor array (PICSA)(Jin et al.,
56 2020), electrical capacitance tomography and venturi tube (Liu et al., 2017), ultrasonic
57 transducers and electrical sensors(Tan et al., 2016), ultrasonic transducer and venturi
58 tube(Huang et al., 2013), and gamma-ray densitometer and electrical conductivity
59 probes (Descamps et al., 2006) have been reported in the literature.

60 In addition, data fusion of several sensor signals and physical model of the multiphase
61 flow for real time measurement of oil, gas and water flow rates in a three phase flow
62 was successfully implemented by Meribout et al., (2010). Similarly, Figueiredo et al.,
63 (2016) reported an oil-continuous multiphase flow measurement method by using
64 acoustic attenuation data for generating data for neural networks model for flow pattern
65 recognition as well as gas volume fraction (GVF) estimation. But the downside of this
66 type of multi-sensor multiphase flowmeters that it first involves features extraction and
67 data training, and it uses invasive sensors which may incur pressure loss and higher
68 installation or retrofit costs.

69 Conductance sensor, even though it is an intrusive device, has been widely used for
70 measuring the phase fraction or the flow velocity of oil-water two-phase flow (Chen et
71 al., 2015). It records the time-varying electrical conductive characteristics of the oil–

72 water flow, However, conductance sensors are significantly affected by phase inversion
73 when flow changes from water-continuous flow to oil-continuous flow, the detection
74 has to change from conductance to capacitance (Figueiredo et al., 2016). In a similar
75 way, electrical capacitive sensors, though non-invasive, are susceptible to coating by
76 paraffin wax and affected by the phase inversion as well, when the flow changes to
77 become conductive as in water continuous-flow (Chaudhuri et al., 2014; Dong et al.,
78 2015). Moreover, turbine flowmeter and Venturi tube are intrusive instruments and so
79 they can cause flow constriction or contribute to pressure losses. A Non-invasive two-
80 phase flowmeter eliminates causes of pressure drop and corrosion of sensor, and
81 importantly, it will help to reduce installation cost and maintenance cost (Kumara et al.,
82 2010a). Ultrasonic Doppler technique is good choice for two-phase flow measurement
83 as it operates without flow disturbance and not restricted by pipeline material(Yin et al.,
84 2019).

85 Ultrasonic techniques have been widely used for both phase velocity and phase fraction
86 measurements (Thorn et al., 2013). The ultrasonic Doppler techniques have been
87 explored for velocity measurement are the pulsed-wave ultrasonic Doppler(PWUD) and
88 continuous-wave ultrasonic Doppler(CWUD) (Tan et al., 2021). PWUD utilises a single
89 transducer to intercept the moving stream by sending short ultrasonic burst and
90 receiving echoes from tracer particle along a sound beam. A typical example of such a
91 sensor is described by (Baker and Yates, 1973; Murai et al., 2010; Yin et al., 2019). The
92 CWUD uses two separate transmitting and receiving transducers to measure the
93 average flow velocity(Abbagani and Yeung, 2016; Brody et al., 1974; Dong et al.,
94 2016, 2015; Tan et al., 2021). Although measurements obtained by PWUD devices are
95 perfectly adequate for flow measurement, maximum flow velocity can be measured

96 with the PWDU is limited by its sampling frequency (Tan et al., 2021). The CWDU
97 technique can accurately measure flow velocity of oil-water two-phase flow and
98 theoretically, there is no maximum limit to the subsonic flow velocity it can measure.

99 In fact, the non-invasive continuous wave Doppler ultrasound (CWDU) system was
100 first invented for medical application in 1957 by Satomura, and in particular, the
101 CWDU sensor is being developed for various flow measurement ever since. Kouame et
102 al., (2003) presented an application of CWDU sensor for two phase flow velocity
103 measurement and proposed the use of high resolution frequency techniques to overcome
104 the problem of coloured noise. Shi et al., (2017) applied CWDU sensor technique to
105 study oil-water flow in horizontal pipe and developed a model which takes into the
106 influence of holdup distribution in determining the overall superficial flow velocity.
107 Dong et al., (2015) developed a method of measuring oil-water two-phase flow using
108 CWDU transducers and a generalised two-phase oil-water flow model. However, there
109 was no consideration of hybrid sound velocity to compensate for the changes in sound
110 velocity in the oil-water mixture flow. This may reduce the accuracy of the method.
111 Similarly, Tan et al., (2016) developed a two-phase oil-water flow measurement model
112 for a combined two sensor system of CWDU transducers and electrical sensors and
113 studied oil–water two-phase flow through horizontal pipe experimentally for estimating
114 the mixture flow velocity.

115 However, oil–water vertical flow measurement using ultrasonic Doppler methods are
116 rather scanty. In order to measure mixture flow velocity of liquid-liquid flow such as the
117 oil-water using the ultrasonic Doppler sensor, a theoretical model would be needed to
118 supplement the CWDU sensor measurements. As examples, such mathematical models
119 have been developed for horizontal oil-water flow in the literatures (Dong et al., 2016,

120 2015; Liu et al., 2021; Tan et al., 2016). Table 1 presents recent experimental works for
 121 oil–water flow measurements. a more elaborate survey over ultrasonic Doppler
 122 methods for multiphase flow measurement can be found in Tan et al., (2021).

123 **Table 1** Recent experimental works for oil–water flow measurement

	Tan et al., (2016)	Mazza and Suguimoto, (2019)	Liu et al., (2021)	Jin et al., (2020)
Oil density, kg/m^3	841	793	790	Not stated
Oil viscosity, (Pa.s)	0.0147	0.0011	0.029	Not stated
Pipe diameter (mm)	50	26	50	20
Pipe orientation	Horizontal	Vertical	Horizontal	Horizontal
Superficial velocities, m/s	Yes	No	No	Yes
Water fraction/holdup measurement	Yes	Yes	No	Yes
Flow pattern identification	No	Yes	Yes	Yes
Sensing device(s)	Ultrasonic sensor	Pressure transducers & conductance/capacitance sensor	Ultrasonic sensor and conductance sensor	Electromagnetic flowmeter and conductance sensor

124
 125 From the table it is clear that only Mazza and Suguimoto, (2019)Mazza and Suguimoto,
 126 (2019) performed experimental oil-water vertical flow measurement but they use
 127 pressure transducers and impedance probes. Jin et al., (2020) Jin et al., (2020)studied
 128 vertical low-velocity oil-water two-phase horizontal flow using electromagnetic
 129 flowmeter and conductance sensor and stated that non-uniform conductivity distribution
 130 leads to error for the output of the EMF. Liu et al., (2021) investigated experimentally
 131 the flow pattern identification of oil-water horizontal flow using ultrasonic transducer

132 and conductance sensor but do not provide holdups and superficial flow velocities. The
133 above-mentioned studies have shown not just the strengths of the ultrasonic Doppler
134 technique but also a necessity for establishing a theoretical model for measurement of
135 oil-water two-phase using the CWDU sensor. However, most of the ultrasonic Doppler
136 methods are limited to horizontal flow and the phase fraction data were obtained with
137 conductance sensor- an intrusive device!

138 Gamma densitometer is also a non-invasive sensing device that is often used in
139 measuring phase volume fraction and mixture flow density (Descamps et al., 2006;
140 Kumara et al., 2010a). Descamps et al., (2006) measured the density of oil–water flow
141 through a vertical tube and in situ liquid (oil and water) hold up, using a Berthold LB
142 444 gamma ray densitometer. Kumara et al., (2010a) experimentally investigated oil-
143 water flow in a 15 m long, 56 mm diameter horizontal and slightly inclined pipes and
144 measured the time averaged cross-sectional distributions of oil and water with by
145 traversing a single-beam gamma densitometer along the vertical pipe diameter.

146 The above survey revealed that the ultrasound Doppler sensor and the gamma-ray
147 densitometer are right choice for a non-invasive multiphase flow measurement system.
148 Experimental results reported in the literatures on the studies of liquid-liquid flow
149 measurement also showed that there is little research available on the use of clamp-on
150 (non-invasive) ultrasonic Doppler method to measure oil-water two-phase flow,
151 especially in the vertical pipe. A Non-invasive technique can be used as a temporary,
152 semi-permanent or permanent method of multiphase flow measurement(Sanderson and
153 Yeung, 2002).

154 Measurement of the phase flowrates is an important part of managing oil production
155 and besides, it is a necessary prerequisite for water disposal and/or water

156 reinjection(Faraj et al., 2015). However, the majority of the studies in oil-water flows
157 are confined to horizontal pipes and the flow patterns in the vertical oil-water two-phase
158 flow are entirely different from that of the horizontal flow systems. The motivation
159 behind the present study is to perform an experimental study on oil-water two-phase in
160 vertical upward flow pipe using non-invasive Doppler ultrasonic methods for
161 measurement of the phase flow rates.

162 In the present study, firstly it is focused on measuring the superficial the mixture flow
163 velocity with the CWDU sensor conjunction with a theoretical flow velocity profile
164 model, and the water volume fraction using the gamma-ray densitometer this paper, a
165 non-invasive method to estimate the mixture flow velocity and The mixture flow
166 velocity encompasses both laminar and turbulent velocity profiles to represent the two
167 main flow regimes of oil-continuous flow and water-continuous flow respectively.
168 Secondly, the drift-flux model will be modified to estimate the superficial flow
169 velocities of oil and of water from the data obtained by measuring the mixture flow
170 velocity and calculating the water volume fraction. The estimated results will be
171 compared with single phase flow meters at the inlets of the test rig. The difference
172 between the test flowmeters and the reference flowmeters will be discussed along the
173 effects of the phase volume fraction on the measurement results.

174

175 **2 Measurement Methodology**

176 **2.1 Ultrasound Doppler principle**

177 A CWDU sensor uses the Doppler effect principle for the of flow measurement, in
178 which both the ultrasound signal transmitter and receiver transducers are stationary but
179 former sends ultrasound waves to and latter receive scattered waves from the moving

180 scatterers (droplets) in the flow. The average the droplets velocity in the measuring
 181 volume of the CWDU flowmeter sensor \bar{v} is determined using the Doppler effect
 182 principle as (Brody et al., 1974; Shi et al., 2017). Details on the interaction of the
 183 ultrasound wave with the oil-water flow can be found in (Dong et al., 2015a; Liu et al.,
 184 2021; Tan et al., 2021; Zhai et al., 2013).

185 The received ultrasound from a point droplet is a sinusoidal signal shifted in frequency
 186 from the transmitted ultrasonic carrier by an amount f_d . The f_d is related to the
 187 classical Doppler shift formula(Brody et al., 1974):

$$\bar{v} = \frac{c\bar{f}_d}{2f_t \cos \theta} \quad (2-1)$$

188 where: c is the speed of sound, f_t is the transmitted ultrasonic carrier frequency, θ is the
 189 transducer orientation angle and \bar{f}_d is the average frequency shift reflected by multiple
 190 droplets in the flow.

191 Although, there are some very small gas bubbles in the oil-water flow which could also
 192 scatter the ultrasound which may complicate the measurement. The present method
 193 assumes that the two-phase flow is well-mixed and the air particles in the flow are
 194 infinitesimally small compared to the wavelength of sound, and the effects of scattering
 195 by gas-bubble is neglected (Chaudhuri et al., 2014; Garcia-Lopez and Sinha, 2008).

196 In oil-water two-phase flow, nevertheless, the Eqn. (2-1) could still be susceptible to
 197 errors due to the different sound speed in oil and in water (Dong et al., 2015). Therefore,
 198 the sound speed in the oil/water mixture is a hybrid sound speed c_{ow} which can be
 199 obtained from the Urick(1947) model, as follows (Garcia-Lopez and Sinha, 2008):

$$c_{ow} = \frac{1}{\sqrt{\rho_m^2 k_m}} \quad (2-2)$$

200 The variables ρ_m and k_m denote the mixture density $\rho_m = \rho_w\alpha_w + (1 - \alpha_w)\rho_o$ and
 201 the mixture compressibility $k_m = k_w\alpha_w + (1 - \alpha_w)k_o$.
 202 where α_w is the phase volume fraction of water , k_w is the compressibility of water and
 203 k_o is the compressibility of oil respectively, and ρ_w and ρ_o denote density of the oil
 204 and the water, respectively.
 205 Equation (2-2) is an appropriate result for estimation of the sound speed in the mixture
 206 flow. Rewriting Eqn. (2-1):

$$\bar{v} = \frac{c_{ow}\bar{f}_d}{2 f_t \cos \theta} \quad (2-3)$$

207 Equation (2-3) shows the expression of the flow velocity under the assumption that the
 208 transducers are uniformly transmitting and receiving ultrasonic signal into and from the
 209 flow and homogeneous distribution of the droplets in the flow. The flow velocity can
 210 computed and subsequently, the average flow rate can be estimated; knowing the cross-
 211 section area of the pipe (Brody et al., 1974).

212 The droplets are travelling at different velocities and the received Doppler signal
 213 contains a distribution of frequencies which can produce a spectrum. So, the Doppler
 214 signal can be analysed through to the spectral estimation. The average Doppler
 215 frequency shift \bar{f}_d was calculated from a power spectrum using an intensity-weighted-
 216 mean (IWM) equation(2-4) (Morriss and Hill, 1991).

$$\bar{f}_d = \frac{\int_0^{f_{max}} P(f) f df}{\int_0^{f_{max}} P(f) df} \quad (2-4)$$

217 where: f_{max} is the maximum Doppler frequency, $P(f)$ is the Doppler power spectrum,
 218 \bar{f}_d is the average Doppler shift, f_t is the transmitted frequency and f is the Doppler
 219 frequency shift

220 The CWDU sensor may be used to measure the flow velocity in the whole pipe cross
221 section. However, the sensing volume of the CWDU sensor is fixed region (often it does
222 not cover the whole pipe cross-section) in the in pipe through which moving droplets
223 will cause a detectable Doppler-shifted signal (Baker and Yates, 1973) A rule of thumb
224 to follow is not to choose ultrasound sensor with measuring volume larger than is
225 necessary. This is to avoid ultrasound signal reflection through the pipe walls which is a
226 major concern. Other constraints include: (1) if the transducer were designed to have
227 bigger dimensions so as to produce larger measuring volume, then the origin of echoes
228 may come from the pipe walls as well. (2) if the if the sample volume is too small only
229 a uniform flow profile (i.e., plug flow) can be accurately measured (Rothfuss et al.,
230 2016). The measurement volume of the present method and pipe diameter is described
231 in the section 3.3. The capability of the CWDU sensor for flow velocity measurement
232 can be improved as described by the recent development of CWDU sensor through a
233 theoretical correlation by Dong et al., (2015a) and Tan et al., (2016).

234 The mean velocity V_m can be estimated by integrating the flow velocity in the
235 measuring volume. Based on these assumptions: (i) the ultrasonic intensity in the
236 measuring volume is homogeneous, and (ii) the distribution of droplets is homogeneous
237 in the measuring volume (Kikura et al., 2004). For oil-water flow measurement using
238 the Doppler measurement effective flow models is necessary to integrate the Doppler
239 shift frequency to handle the complex flow distribution (Tan et al., 2021). For example,
240 .Dong et al., (2015) carried out experiments with oil-water two-phase flow in a
241 horizontal pipe and used a mathematical Doppler model for combining the flow velocity
242 profile and the measured flow velocity in the measuring volume for measuring the
243 mixture flow. suggested a boundary layer model for describing the velocity profile of

244 dispersed and stratified oil-water flow for predicting superficial flow velocity and the
245 flow velocity profile, measured flow velocity by ultrasonic sensor and phase fraction
246 data were all combined to the predict the superficial flow velocity of each phase.
247 Measurement of superficial flow velocities of oil and water in oil-water vertical pipe
248 was not included in their work. In another development, Dong et al., (2016) described a
249 method of incorporating the mathematical Doppler model (described in (Dong et al.,
250 2015)) into the drift-flux model, based on the assumption that there is slippage between
251 two phases, and the they found that the overall measurement error was reduced by
252 2.27%. However, these studies were conducted in horizontal pipes, and besides, the
253 phase fraction was measured with electrical conductance sensor. Therefore, we extend
254 that the method of mathematical Doppler model with the ultrasonic Doppler sensor for
255 estimating the mixture oil-water flow to include estimation of the superficial flow
256 velocity of oil and water from the measured mixture flow velocity.

257 **2.2 Gamma ray densitometry**

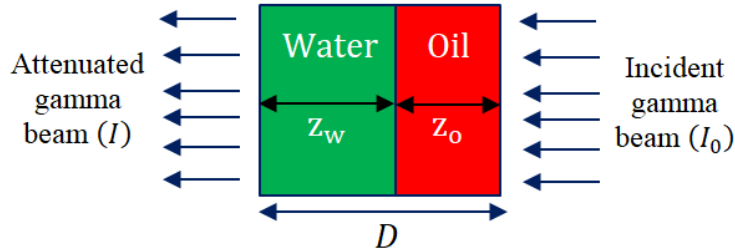
258 The gamma ray densitometer measurement theory is based upon electromagnetic
259 radiation passing into the material is received by a detector. The emission and reception
260 of the gamma electromagnetic radiation is governed by the Beer–Lambert’s law
261 (Kumara et al., 2010a):

$$I = I_0 \exp(-\varphi z). \quad (2-5)$$

262 where I_0 is the initial intensity, (photon/m² – sec) , φ is the linear absorption
263 coefficient; z is the distance travelled through the absorbing medium and I is the
264 intensity of the gamma beam received at the detector.

265 Falcone et al., (2009) described a model of attenuation of gamma radiation across the
266 pipe filled up with a multiphase flow for deriving the expression for the phase volume

267 fractions. The multiphase flow in a pipe is modelled as a square channel filled with oil
 268 and water with oil-water two-phase as shown in Figure 2-1(Kumara et al., 2010a; Stahl
 269 and von Rohr, 2004). a similar methodology for the for derivation of the expression for
 270 the phase volume fractions is adopted here.



271

272 **Figure 2-1** Attenuation of gamma radiation in a square channel filled with oil and water
 273 Assume that there are two phases in the channel (e.g. oil and water) with path lengths
 274 for the gamma beam traversing the respective phases of z_o and z_w . The intensity I of
 275 the gamma beam received at the received at the detector is given by:

$$I = I_0 \exp(-\varphi_p z_p) \exp(-\varphi_a z_a) \exp(-\varphi_w z_w) \exp(-\varphi_o z_o) \quad (2-6)$$

276 where φ_p = linear absorption coefficient in the tube wall material; z_p = path length
 277 through wall; φ_a = linear absorption coefficient for air; z_a path length through air; φ_o ,
 278 and φ_w = linear absorption coefficient for oil and water phases respectively.

279 For the two-phase mixture, the common method of calibrating the gamma densitometer
 280 is to measure the intensities (I_o and I_w) when the channel is full of each respective
 281 phase. Thus,

$$I_o = I_0 \exp(-\varphi_p z_p) \exp(-\varphi_a z_a) \exp(-\varphi_o D) \quad (2-7)$$

282

$$I_w = I_0 \exp(-\varphi_p z_p) \exp(-\varphi_a z_a) \exp(-\varphi_w D) \quad (2-8)$$

283 Normally, the absorption in air is negligible.

284 Referring to Eqns. (2-6), (2-7) and (2-8), these give the test volume fractions for
 285 perpendicular phase distribution along the path length of the gamma beam as:

$$\alpha_o = \frac{z_o}{D} = \frac{\ln(I/I_w)}{\ln(I_o/I_w)} \quad (2-9)$$

286

$$\alpha_w = \frac{z_w}{D} = \frac{\ln(I/I_o)}{\ln(I_w/I_o)} \quad (2-10)$$

287 **2.1 Two-phase flow regime models**

288 Oil–water two-phase flow can be grouped into 1) the water continuous flow and 2) the
 289 oil continuous flow based on the flow rates and phase volume fraction. In oil-water two-
 290 phase flow, the Reynolds numbers of water-continuous flow is high and presumably
 291 turbulent flow but most oil continuous flow has a low Reynolds number and it is
 292 assumed that the flow will be laminar(Dong et al., 2015).

293 **2.1.1 Laminar flow velocity profile**

294 For a laminar vertical flow, the mean velocity(V_m) and its maximum velocity(V_{max})
 295 and the parabolic solution for laminar flow velocity profile($u(r)$) in circular pipe can
 296 be expressed as:

$$u(r) = -\frac{R^2}{4\mu} \left(\frac{dP}{dx} + \rho_m g \sin \Phi \right) \left(1 - \frac{r^2}{R^2} \right) \quad (2-11)$$

$$V_m = \frac{2}{R^2} \int_0^R u(r) r dr = -\frac{R^2}{8\mu} \left(\frac{dP}{dx} + \rho_m g \sin \Phi \right) \quad (2-12)$$

$$V_{max} = -\frac{R^2}{4\mu} \left(\frac{dP}{dx} + \rho_m g \sin \Phi \right) \quad (2-13)$$

297 where y is the distance from the pipe centreline, R is the pipe radius, μ is the flow
 298 viscosity, $\frac{dP}{dx}$ is the axial pressure gradient, ρ_m is the mixture density, g is the

299 acceleration due to gravity and ϕ is the angle of inclination of the flow pipe from the
300 horizontal.

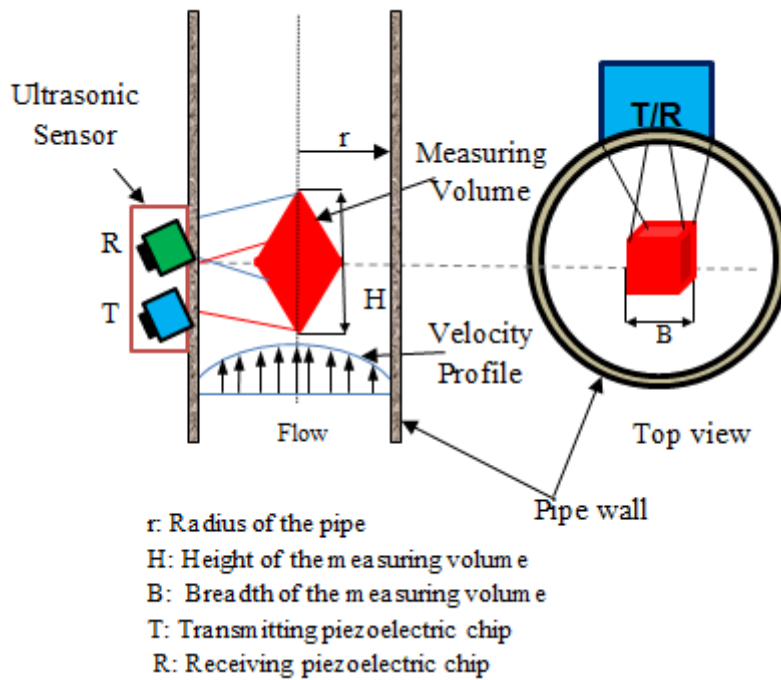
301 For oil-continuous flow measurement, (V_{o-m}), is the mean velocity, and (V_{omax}) is its
302 maximum velocity. The mean velocity in the measuring volume \bar{v} can again be
303 expressed as in Eqn.(2-12)

$$\bar{v} = \frac{\int_0^r \left(1 - \frac{y^2}{R^2}\right) 2\pi y dy}{\pi r^2} \cdot V_{omax} = V_{omax} \left(1 - \frac{\sigma^2}{2R^2}\right) \quad (2-14)$$

304 where σ is the radius of the measuring volume

305 Equation (2-3) is for the calculation of the local velocity which is the average velocity
306 of the scatterers in the measuring volume. The CWDU sensors can only measure the
307 local velocity directly but not the true mean flow velocity. However, the mean velocity
308 can be determined by establishing a theoretical relationship between the local flow
309 velocity and the flow velocity profile. The measuring volume of a CWDU sensor is a
310 fixed region in the flow pipe where the transmitting and receiving ultrasound beams
311 intersect as a result of a presence of detectable moving scatterers (Baker and Yates,
312 1973; Rothfuss et al., 2016). Figure 2-2 shows the relationship between the measuring
313 volume and flow. The measuring volume shape and size is determined by the
314 dimensions of the piezoelectric chip and the geometry of the intersections of transmit
315 and receive ultrasound beams as suggested by Dong et al., (2015a).

316



317

318 **Figure 2-2** Relationship between the flow and the measuring volume

319 The mean velocity of the flow laminar oil-continuous flow in across the flow pipe is
 320 expressed as

$$V_{o-m} = \frac{\int_0^R \left(1 - \frac{y^2}{R^2}\right) 2\pi y dy}{\pi R^2} \cdot V_{omax} = \frac{1}{2} V_{omax} \quad (2-15)$$

321 Eliminating the maximum velocity, V_{omax} between these two equations (2-14) and
 322 (2-15) gives an equation of the mean velocity of oil-continuous laminar flow V_{o-m}

$$V_{o-m} = \frac{R^2}{(2R^2 - \sigma^2)} \cdot \bar{v} \quad (2-16)$$

323 **2.1.2 Turbulent flow velocity profile**

324 In addition to the laminar flow profile described above, the importance of the role
 325 played by turbulence in oil-water two-phase flow cannot be over emphasized. As an
 326 example, Hu et al., (2007) studied oil-water vertical dispersed flow in 38mm ID pipe to
 327 investigate the crucial role of the turbulence in the distribution, and mixing of the
 328 phases and its contribution in droplet/bubble formation and breakage. They found out

329 that the phase fraction and the velocity of the dispersed both affect the characteristics in
 330 oil-water flow. Moreover, Paolinelli, (2020) proposed a mechanistic model for stability
 331 of dispersed oil-water flow in horizontal and inclined pipes and the h the model was
 332 tested to be able to predict the break-up of dispersed phase droplets, and accumulation
 333 of droplets.

334 In this work, we present an investigation on turbulent flow regime as well. Velocity
 335 distribution in a pipe of a turbulent-flow can be resolved by either using the power law
 336 or from the logarithmic law. In the present study, the properties of the water-continuous
 337 turbulent flow velocity profile is by application of the logarithmic-law because it is very
 338 often in agreement with experimental data (Chemlou et al., 2009; Eskin et al., 2017;
 339 Kumara et al., 2010c). The logarithmic-law for the velocity profile can be expressed as

$$u^+ = 2.5 \ln y^+ + 5.5, \quad y^+ > 11.6 \quad (2-17)$$

340 In the analysis of turbulent velocity profiles using the logarithmic law of the wall, it is
 341 easier to work with non-dimensionalised variables: y^+ is a non-dimensionalised distance
 342 defined as $y^+ = \frac{u_\tau y \rho_m}{\mu_m}$ and u^+ is a non-dimensionalised velocity and it is defined
 343 as: $u^+ = u/u_\tau$, where u_τ is the shear velocity and it is defined in section 2.1.2.1. For a
 344 circular pipe, $y = R - r$, where R is the pipe radius and r denotes the radial position
 345 where the velocity is calculated, and y is the radial distance from the pipe wall.

346 Substituting the non-dimensionalised variables into Eq. (2-17), the Logarithmic-law
 347 layer velocity profile of turbulent oil-water two-phase flow in a pipe can be expressed
 348 as:

$$u_{ow} = 2.5 u_\tau \ln \left[\frac{(R - r) u_\tau \rho_m}{\mu_m} \right] + 5.5 u_\tau \quad (2-18)$$

349 where u_τ is the shear velocity

350 2.1.2.1 Shear velocity model

351 The shear velocity u_τ can be expressed in terms of the wall shear stress and the
352 mixture density.

$$u_\tau = \sqrt{\tau_w / \rho_m} = \sqrt{\frac{D}{4\rho_m} \cdot \frac{dP}{dx}} \quad (2-19)$$

353 where τ_w is the shear stress at the pipe wall, ρ_m is the density of oil-water mixture D is
354 the pipe's internal diameter and $\frac{dP}{dx}$ is pressure gradient

355 For fully developed flow, the total pressure gradient is the sum of the frictional pressure
356 gradient, and the gravitational pressure gradient (Brauner, 2002; Rodriguez and
357 Oliemans, 2006):

$$\frac{dP}{dx} = 2f_m \frac{\rho_m V_m^2}{D} - \rho_m g \sin \Phi \quad (2-20)$$

358 where V_m is the mixture flow velocity, f_m the Fanning's friction factor of the two-phase
359 mixture and g is acceleration due to gravity.

360 The friction factor f_m can be estimated from a correlation given the fluid properties such
361 as Reynolds number, mixture flow velocity, viscosity and density. For turbulent flow of
362 Newtonian fluids, the friction factor can be obtained from the Moody diagram, or
363 calculated from one of the experimental correlations such as the Colebrook equation and
364 Blasius correlation suggested in the literature (Brauner, 2002; Descamps et al., 2006).

365 The Moody diagram is accepted and used charts in engineering but the pipes roughness
366 may increase with use as a result of corrosion, scale build-up, and precipitation.
367 Consequently, the friction factor may augment by a factor of 5 to 10 (Çengel, 2007).
368 Similarly, Colebrook combined the data for transition and turbulent flow in both smooth
369 and rough pipes into the following implicit relation known as the Colebrook equation:

$$\frac{1}{\sqrt{f}} = -2.0 \log \left(\frac{\varepsilon/D}{3.7} + \frac{2.51}{Re\sqrt{f}} \right) \quad (2-21)$$

370 The Colebrook equation is equivalent to the Moody chart (Çengel, 2007). In addition,
371 the Blasius correlation in smooth tubes is given as:

$$f_m = \frac{b}{Re^n}, \quad 300 \leq Re \leq 100,000 \quad (2-22)$$

372 Coefficient b and exponent n are to be obtained experimentally so as to fit experimental
373 pressure drop data. The Re is Reynolds number Re for two-phase flow is to be defined
374 in section 3.6

375 In the literature, there are several correlations for the effective viscosity of liquid–liquid
376 two-phase flow but those different expressions seem to have little impact on the
377 homogenous model predictions because there are other factors involved (Grassi et al.,
378 2008). Therefore, the effective viscosity μ_m for the oil-water flow was calculated using
379 as the expression in the Eqn. (2-23) (Dong et al., 2015; Kumara et al., 2009; Tan et al.,
380 2016).

$$\mu_m = \alpha_w \mu_w + \alpha_o \mu_o \quad (2-23)$$

381 where μ_w and μ_o are the dynamic viscosities of water and oil respectively.

382 The mixture density, ρ_m , of the oil-water flow can be determined from the gamma-ray
383 densitometer. From phase fraction can then be determine by

$$\rho_m = \rho_w \alpha_w + (1 - \alpha_w) \rho_o \quad (2-24)$$

384 Substituting frictional pressure gradient and mixture density into the Eq. (2-19) produces
385 Eqn.(2-25), hence the Shear velocity for the mixture vertical flow is

$$u_\tau = \sqrt{\left(\frac{D}{4\rho_m} \right) \cdot \left[2 \left(\frac{b}{Re^n} \right) \frac{\rho_m V_m^2}{D} - \rho_m g \right]} \quad (2-25)$$

386 **2.1.2.2 Determining the mixture flow velocity**

387 The relationship between the average velocity of the flow droplets \bar{v} and the shear
 388 velocity u_τ is obtained by integrating the velocity profile over the area of the pipe.

389 Therefore,

$$\bar{v} = \frac{\int_0^R u_{ow} \cdot 2\pi r dr}{\pi R^2} \quad (2-26)$$

390 where u_{ow} is the oil-water flow velocity profile. Again by substituting Eqn. (2-18) into
 391 Eqn.(2-26)we have

$$\bar{v} = \frac{1}{\pi R^2} \int_0^R u_\tau \left[2.5 \ln \frac{(R-r)u_\tau \rho_m}{\mu_m} + 5.5 \right] 2\pi r dr \quad (2-27)$$

392 Obviously the integration of Eqn. (2-27) is cumbersome to process. However, the
 393 equation can be easily integrated by using a computer program such as
 394 ‘*MATHEMATICA*’ to obtain a numerical solution as (Kudela, 2010).

$$\bar{v} = \frac{1}{2} u_\tau \left(\frac{2}{k} \ln \frac{u_\tau \rho_m R}{\mu_m} + 2B - \frac{3}{k} \right) \approx 2.5 u_\tau \ln \frac{u_\tau \rho_m R}{\mu_m} + 1.75 u_\tau \quad (2-28)$$

395 Equation (2-28) shows the relationship between the shear velocity u_τ and the average
 396 velocity of the flow droplets \bar{v} . Solving Equation (2-28) we obtain a formula relating
 397 the shear velocity u_τ to the average velocity of the flow droplets \bar{v} (One exemplary
 398 solution is given in the Appendix A),. The value of the shear velocity u_τ of each test
 399 point obtained from the average velocity of the flow droplets \bar{v} which are substituted
 400 into the Eqn.(2-29) to estimate the mixture flow velocity V_m .Solving Eqn.(2-25) for V_m
 401 and let the mixture flow velocity in the water-continuous flow be($V_m = V_{w-m}$):

$$V_{w-m} = \left[\left(\frac{4u_\tau^2 + Dg}{2b} \right) \cdot \left(\frac{\rho_m D}{\mu_m} \right)^n \right]^{\frac{1}{2-n}} \quad (2-29)$$

402 The coefficient b and exponent n can be adjusted to fit friction data better according to
403 the Reynolds number each data in the test matrix. Besides, constant coefficients cannot
404 accurately represent all ranges of turbulent flow (Dong et al., 2016).

405 **2.2 Individual phase flow rate by the drift-flux model**

406 The flow velocities of oil and water phases in oil-water two-phase are different because
407 of the slip existing between the continuous phase and the dispersed phase. So, it is
408 important to estimate each phase flow velocity. However, superficial flow velocities of
409 oil and of water cannot be directly measured downhole. Therefore, it is necessary to
410 have a model of oil-water two-phase which allows allow prediction of these flow rates
411 from flow properties that can be measured in the well(Lucas and Jin, 2001).

412 The Zuber-Findlay (1965) drift flux model, which was originally developed for gas-
413 liquid two-phase flow, has been modified to model the relationship between the oil
414 flow velocity($\frac{V_{so}}{\alpha_o}$) and the mixture flow velocity(V_m) by several authors (Dong et al.,
415 2016; Du et al., 2012; Hasan and Kabir, 1998; Mazza and Suguimoto, 2019). The drift-
416 flux can be express as follows:

$$\frac{V_{so}}{\alpha_o} = C_o V_m + U_{ow} \quad (2-30)$$

417 where α_o is the oil phase fraction, V_{so} and V_m are the oil superficial velocity, the
418 mixture flow velocity, C_o is the distribution parameter and U_{ow} is the drift velocity of
419 the dispersed phase.

420 Additional relationships are required for calculating the parameters of the drift-flux
421 model(U_{ow}) and (V_{∞}). Du et al., (2012), Hasan and Kabir, (1998) and Lucas and Jin
422 (2001) have reported extension of the semi-theoretical correlation of Wallis (Wallis,

423 1969) to establish a relationship for the drift velocity(U_{ow}) for oil-water two-phases flow
424 as:

$$U_{ow} = V_{\infty}(1 - \alpha_o)^m \quad (2-31)$$

425 where V_{∞} is the terminal rise velocity of a single oil droplet of the dispersed phase
426 relative to the continuous phase, α_o is the oil volume fraction and m is the exponent
427 drift velocity model.

428 Hasan and Kabir, (1998) first suggested for inclined oil–water two phase flow as $m =$
429 2 . In other previous studies, it was suggested that the exponent can be set as $m =$
430 2 (Du et al., 2012; Lucas and Jin, 2001). In the present study, m is equally selected as 2
431 for both equations. (2-31) and then use the Harmathy correlation which can be
432 expressed as equation (2-32), (Harmathy, 1960), is often used for calculating the
433 terminal velocityvelocity V_{∞} .

434

$$V_{\infty} = 1.53 \left[g \sigma_{ow} \frac{\rho_w - \rho_o}{\rho_w^2} \right]^{1/4} \quad (2-32)$$

435 where σ_{ow} is the oil/water interfacial tension, g is the acceleration of gravity.

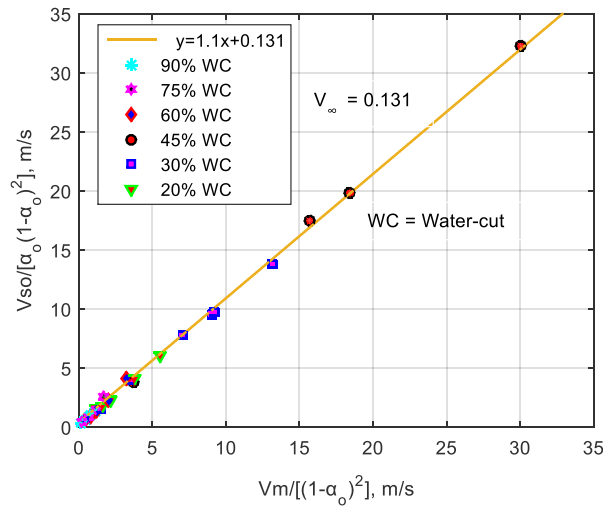
436 By substituting the flow parameters -the densities of the water ρ_w 998.4 kg/m³ and oil
437 ρ_o 815 kg/m³ oil-water surface tension is $\sigma_{ow} = 0.029$ N/m into Eqn. (2-32), the value
438 of $V_{\infty} = 0.131$ (m/s) obtained from the equation(2-32)

439 It can be seen that in the Eqn. (2-32), the drop size is not included into the expression
440 because of the known fact that under turbulent flow conditions the terminal velocity of
441 liquid particles moving in liquid media is practically independent of the particle
442 size(Harmathy, 1960).

443 To determine the value of the distribution parameter C_o , we substitute, V_∞ , V_{so} , V_m and
 444 α_o into Eqn. (2-30) for expressing the general drift-flux equation as:

$$\frac{V_{so}}{\alpha_o(1 - \alpha_o)^2} = C_o * \frac{V_m}{(1 - \alpha_o)^2} + V_\infty \quad (2-33)$$

445 The volumetric flow rates of oil (Q_o) and water (Q_w) flowing into the working section
 446 were measured at the inlets with the single phase flow meters. The reference superficial
 447 velocities of oil and of water were obtained the single phase flow rate using the
 448 expression $V_{so} = (Q_o/A_p)$ and $V_{sw} = (Q_w/A_p)$ respectively. The reference mixture
 449 flow velocity is the sum of the two superficial velocities, $V_m = V_{sw} + V_{so}$. The mean
 450 volume fraction α_o of the oil in the working section was determined from the gamma
 451 densitometer measurements. The distribution parameter (C_o), can be estimated by
 452 plotting the quantity $V_{so}/\alpha_o(1 - \alpha_o)^2$ against $V_m/(1 - \alpha_o)^2$ as it would be expected
 453 from equation (2-33) that the data would fall on a straight line with slope $C_o = 1.1$ and
 454 intercept $V_\infty = 0.131$ as shown in Figure 2-3.



455
 456 **Figure 2-3** $V_{so}/\alpha_o(1 - \alpha_o)^2$ versus $V_m/(1 - \alpha_o)^2$ for vertical upward flow.

457 This is in a good agreement with the value of the distribution parameter reported in the
 458 literatures (Hasan and Kabir, 1998; Picchi et al., 2015).

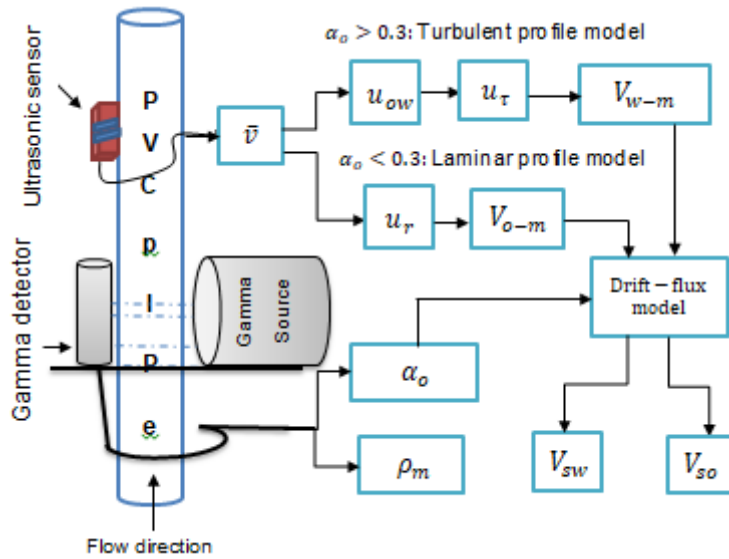
459 The estimated mixture flow velocity of either the oil-continuous flow or the water-
460 continuous flow can be used to predict the the superficial velocity of oil and of water as
461 follows:

$$V_{so} = \alpha_o [C_o V_m + U_{ow}] \quad (2-34)$$

$$V_{sw} = V_m - V_{so} \quad (2-35)$$

462 **2.3 Overall estimation procedure**

463 A schematic diagram of the measurement concept for two-phase oil-in-water flow is
464 illustrated in Figure 2-4. The CWDU flow sensor estimate the average velocity of the
465 droplets (dispersed phase) using Eqn. (2-1). The gamma-ray densitometer was used for
466 measuring the phase fraction of oil in the mixture flow, and subsequently, the mixture
467 density is calculated using equations (2-9) and (2-24) respectively. For oil continuous
468 flow, the velocity profile follows the behaviour of laminar flow and the mean flow
469 velocity can be estimated based on the equation (2-16). Whereas, for the water-
470 continuous flow which has turbulent velocity profile, the flow velocity is estimation by
471 substituting the values of the mixture density, viscosity, shear velocity, pipe diameter
472 and acceleration due to gravity into Eqn. (2-29). Subsequently, the drift-flux model is
473 applied to calculate the individual phase velocities from the overall flow velocity and
474 the phase fraction estimates with Eq. (2-34) and (2-35).



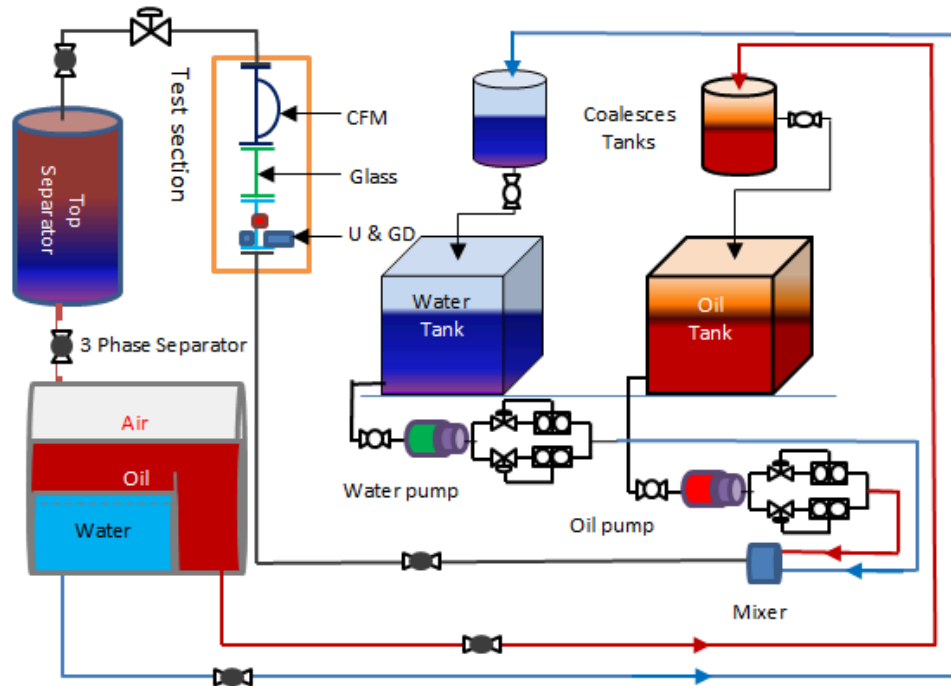
475

476 **Figure 2-4** Combined systems of the CWDU sensor and gamma densitometer for
 477 measurement of two-phase oil-water flow

478 **3 Experimental setup**

479 **3.1 Flow facility, apparatus and test fluids**

480 The experimental investigations to measure vertical up flow of oil-water two-phase flow
 481 were conducted in a multiphase flow test rig at Cranfield University, Bedfordshire,
 482 United Kingdom. Figure 3-1 shows a schematic representation of the multiphase flow
 483 test rig. The flow facility consists of the test rig, water tank, oil tank, a separator, two
 484 centrifugal pumps and measuring equipment. The experimental pipeline is a 2" schedule
 485 10 stainless steel pipeline consisted of an entry length of 40.0m long horizontal and 10.5
 486 m high vertical to ensure enough development length is allowed for the flow. A
 487 transparent PVC pipe test section of 1.2 m long and 50.8 mm i.d. is provided for clear
 488 observation of the flow phenomena at approximately 8.5 from the riser base. At the exit
 489 of the test section, there is a pipe length of 0.60 m to avoid any flow disturbance in the
 490 test section.



491

492 **Figure 3-1** Schematic diagram of the test facility

493 **3.2 Experimental procedure**

494 Process management software (Emerson DeltaV) provided digital automation to the
 495 operation of the test rig (process plant) which allowed for setting the input water and oil
 496 flow rates, and selection of the appropriate pumps and flowmeters. Two separate
 497 dedicated PCs, one with a LabVIEW® for the CWDU sensor and the other with
 498 Chastotomer® software for the gamma densitometer are used for the data acquisitions.
 499 In addition to the two PCs for measurement systems, another PC with LabVIEW
 500 software program is used for recording all the data from the reference instruments. The
 501 test fluids used in the experiments are tap water (density of 998.4 kg/m^3 and viscosity of
 502 $0.001 \text{ Pa}\cdot\text{s}$ at 21°C) and dyed mineral-dielectric oil (Rustlick EDM-250, density of
 503 815 kg/m^3 and a viscosity of about 7.2 mPa at 21°C). The oil flow and water flow were
 504 pumped individually from their storage tanks (12.5 m^3 capacity) into the rig pipeline
 505 through a Y-mixer-manifold, first into the horizontal pipe and then flowed up to the

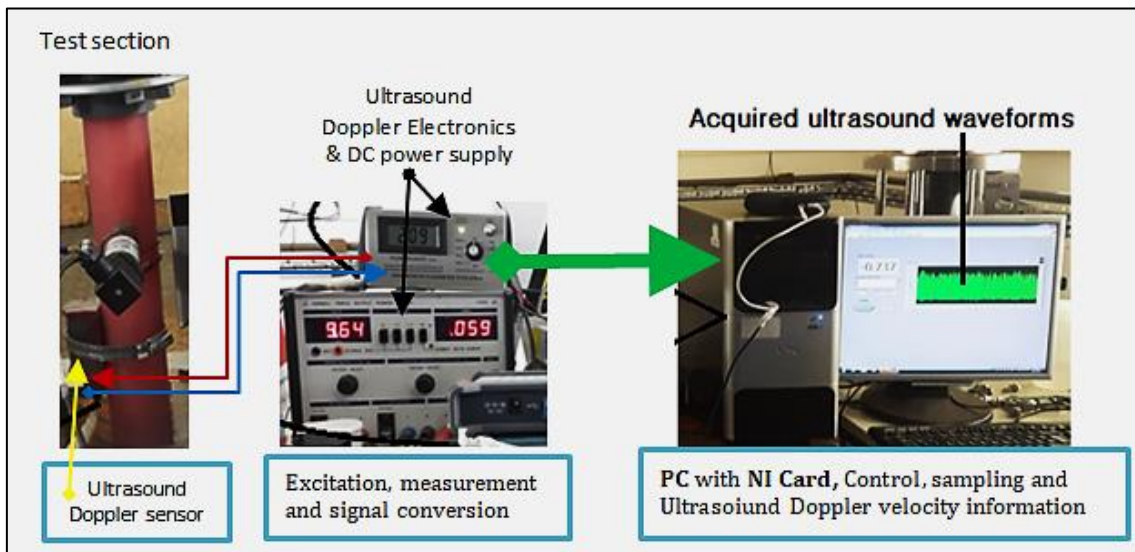
506 vertical pipe section. The oil flow was metered by the reference Micro Motion Mass
 507 flowmeter and a Foxboro Coriolis meter while the water flow was metered by the
 508 reference a Rosemount flowmeter and a Foxboro CFT50 Coriolis meter before the two
 509 liquids were mixed prior to the test section.

510 A Coriolis mass flowmeter (Endress and Hauser Promass 83F) was installed at top of
 511 the test section at approximately 11.0 m from the riser base to measure the oil-water
 512 mixture mass flow and density as a reference density meter. All the reference
 513 flowmeters were, prior to the experimental study, calibrated against a primary reference.
 514 The specifications and operating ranges of the reference flowmeters are given in Table
 515 1.

516 Table 2 Details of instruments of the flow rig

Instruments	Items	Manufacturer	Model	Range	Error (of the span)
Coriolis Flowmeter	Oil flow	Micro Motion	F200	up to 1.0 kg/s	$\pm 0.2\%$
Coriolis Flowmeter	Oil flow	Foxboro	CFT50	up to 10.0 kg/s	$\pm 0.10\%$
Coriolis Flowmeter	Water flow	Foxboro	CFT50	up to 10.0 kg/s	$\pm 0.10\%$
EM Flowmeter	Water flow	Rosemount	8742C	up to 1.0 kg/s	$\pm 0.5\%$
Coriolis Flowmeter	Mixture flow	Endress and Hauser	Promass 83F	0 to 50.0 kg/s	$\pm 0.10\%$

517

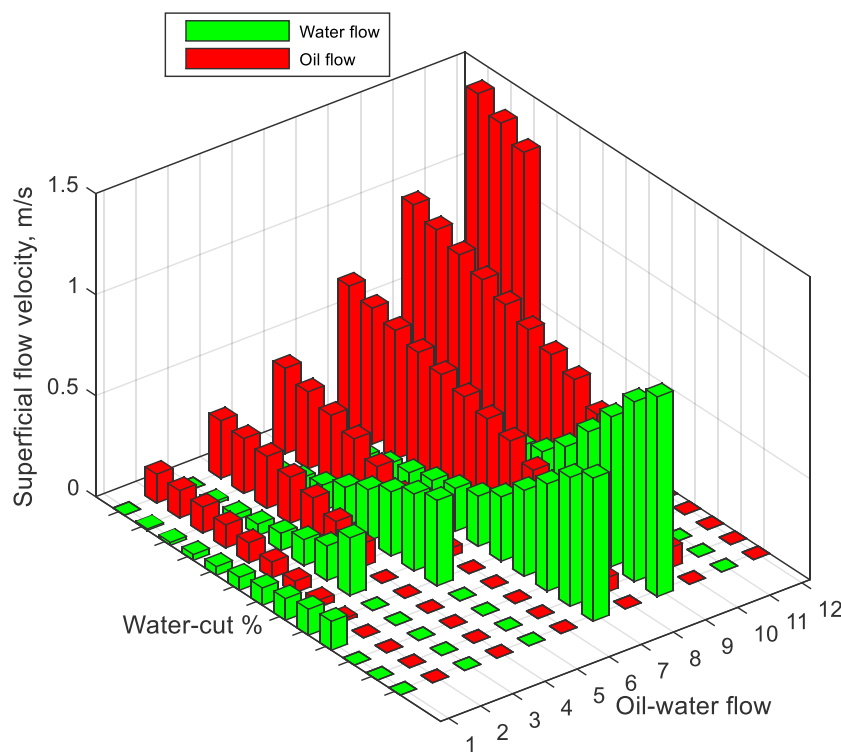


518

519 **Figure 3-2** Oil-water flow test section showing the CWDU sensor set up

520 The water cut is defined as the ratio between the water and total volumetric flow rates as
521 introduced to the inlet section (Ibarra et al., 2017). The flow velocities at the inlet of the
522 rig were calculated as: superficial velocity of the water flow $V_{sw} = Q_w / \rho_w A_p$ and the
523 oil superficial velocity $V_{so} = Q_o / \rho_o A_p$ with A_p being the cross-sectional area of the
524 pipe, $A_p = \pi D^2 / 4$. The flow rates are varied from 0.28 kg/s to 2.78 kg/s (1m³/h to
525 10 m³/h). For each experimental run, the inlet water cut, WC, was varied between 20%
526 and 90% while the total flow velocity, V_m , was kept constant. Surely, this creates two
527 categories of flow: water-dominated flow or oil-dominated flow. However, the drift
528 velocity model can be applied to either status of the continuous phase. This is because
529 the terminal rise velocity of a single droplet of the disperse phase is relative to the
530 continuous phase (Lucas and Jin, 2001). Importantly, the variation of the water-cut has
531 allowed us to observe of flow velocity measurements while the water cut being changed
532 at constant total flow velocity.

533 A wide range of flow rates for mixture flow at different water-cut were measured to
 534 collect a maximum amount data. The test matrix of the data is shown in Figure 3-3. All
 535 test runs were performed at near atmospheric pressure and at a temperature of 21 ± 2
 536 °C. After the mixture flows pass through the test section, it then entered into the
 537 separation equipment which comprises gravity separators and coalesce-tanks. The
 538 mixture flow undergoes separation process and then flow flowed directly into their
 539 respective storage tanks after for re-use.



540

541 **Figure 3-3** Graphical illustration of the test matrix

542 **3.3 CWDU flow sensor instrumentation**

543 The ultrasonic Doppler flow sensor (United Automation Ltd, Southport, UK) has 0.5-
 544 MHz centre frequency and contains a co-housed two piezoelectric chips (*viz*: T and R) T
 545 is for transmitting of ultrasonic waves into the flow and the R for receiving the signals
 546 from the scatterers. Therefore, the measurement volume of the present CWDU sensor
 547 has a square-shape determined by the effective diameters (20mm×20mm) of each

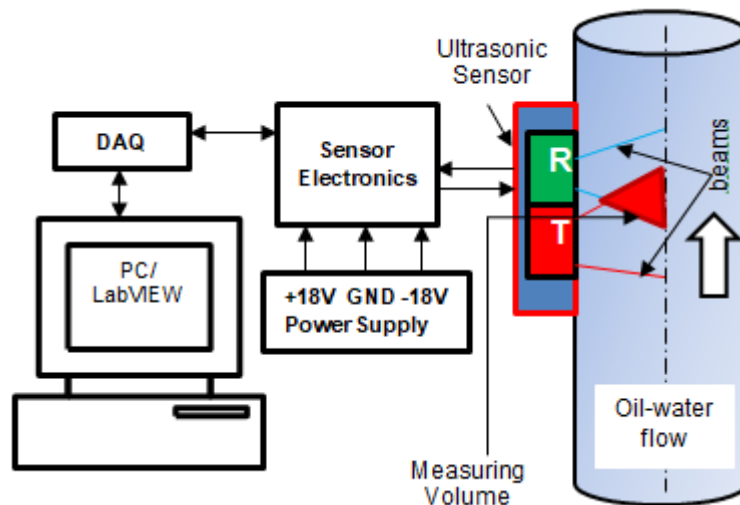
548 element. The sensor was bounded onto the side of the test section pipe using a clip and a
 549 gel to give a firm grip and better contact between the sensor and pipe wall and then it
 550 was connected to a signal conditioning electronic circuit which provided both the
 551 excitation voltage of the transmitting Doppler piezoelectric chip and facilitation of the
 552 data acquisition.

553 In the present study, the excitation voltages of the transmitting Doppler flow meter
 554 sensor were +18v and -18v (36v peak-peak). Table 2 shows the material used in the
 555 experiments and their related acoustic velocity. Figure 3-4 shows a schematic CWDU
 556 sensor system

557 Table 3 physical properties of the material considered

Material	Speed of sound (m/s)	Density (kg/m ³)
Water (20°C)	1484	998.4
Oil (20 °C)	1324	815.4
PVC	2380	1380
Stainless steel	5790	7890

558



559

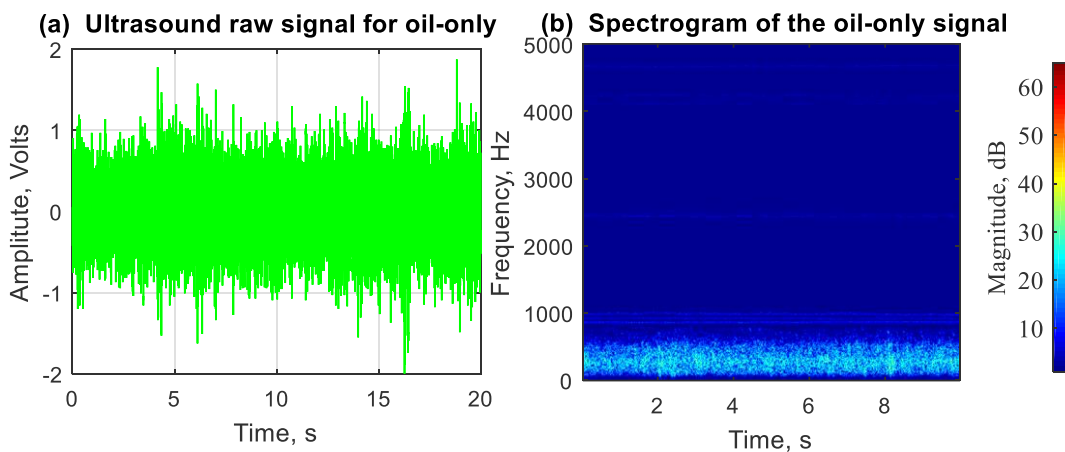
560 **Figure 3-4** a schematic diagram of the CWDU sensor system

561 The Doppler signals were recorded continuously for 20 s at a sampling frequency of 10
562 kHz which is long enough for the flow regime profile to pass through the test section
563 (Zhai et al., 2013). The recorded signal was passed through an anti-aliasing filter and
564 digitized using a computer-based ADC card (NI E-series card PCI-MIO-16E-4, National
565 Instruments, Austin, TX, USA), and recorded onto a hard drive of a PC. The entire data
566 acquisition process is controlled using graphical programming language LabVIEW 10
567 software.

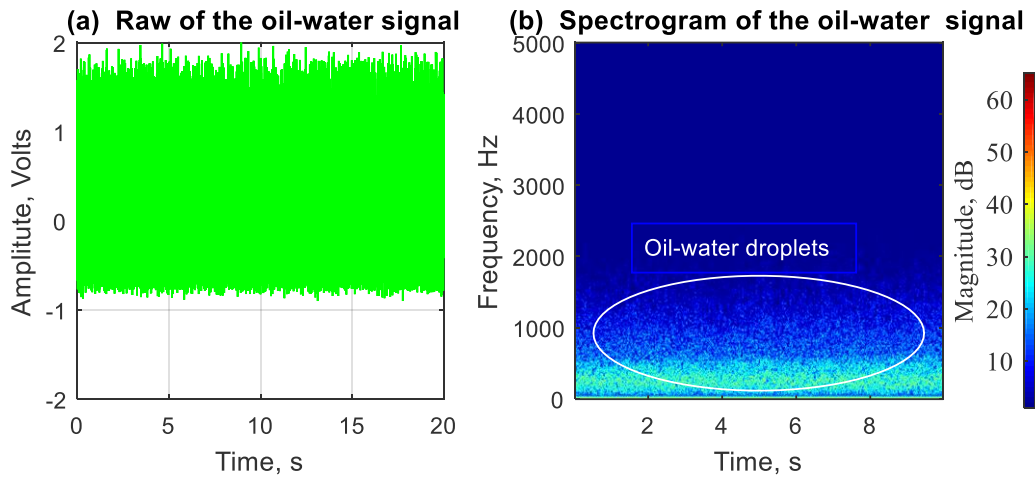
568 The recorded Doppler signal was processed off-line using MATLAB (The Math Works,
569 Natick, MA, USA) on a Windows 7 workstation) for obtaining the mean frequency shifts
570 using an intensity-weighted-mean(IWM) equation(Morriss and Hill, 1991). The flow
571 velocity is calculated using the estimated mean frequency shifts and the sound speed in
572 the fluid. The literature values used as the sound speed and density were 1484 ms^{-1}
573 and 998.4 kg/m^3 for water respectively and corresponding values in the oil were 1324
574 ms^{-1} and 815.4 kg/m^3 respectively(Onda, 2003).

575 Many techniques exist to compute the Doppler spectrum efficiently, based on FFT for
576 example. Liu et al., (2021) reported an application of the FFT algorithm for Doppler
577 spectrum of oil-water flow ultrasound Doppler for flow pattern identification and the
578 authors also demonstrated that the non-invasive CWDU sensor is suitable for both flow
579 velocity measurement and flow patterns identification.. In the present study, the
580 digital signal processing of the ultrasound Doppler signal consists of two parts: fast
581 Fourier transform (FFT) algorithm and intensity weighted mean (IWM) estimation.
582 Firstly, the data series is decomposed into a series of signal in the form of framed with
583 the powers of 2 and windowing to evaluate the frequency spectrum. The windowing

584 technique prevented unwanted frequency appearing in the spectrum. Secondly, with the
 585 FFT, the spectrogram yield instantaneous frequencies as functions of time that give
 586 sharp higher amplitude for the signal reflected off the droplets(Case et al., 2013).
 587 Figure 3-5 and Figure 3-6 are taken from the test data points and they show the logged
 588 raw ultrasonic signal and its Doppler spectrogram calculated using short time Fourier
 589 transform(STFT). The STFT plot or the spectrogram displays distribution of the
 590 frequency shifts in the oil-water two-phase flow. In the case of Figure 3-6, the
 591 spectrogram displays signal strength by colour intensity. Doppler shift frequency is
 592 relatively low and in the present study it ranges between 60Hz and 800Hz and the low
 593 frequency components in the spectrogram are not noise. So, they will not affect the
 594 measurement results.
 595
 596



597
 598 **Figure 3-5** Example of the continuous wave ultrasound signal and its: (a) Raw signal,
 599 and (b) STFT, for conditions: $V_m = 1.25$ m/s, $WC = 0\%$, and a 10kHz signal acquisition
 600 frequency.



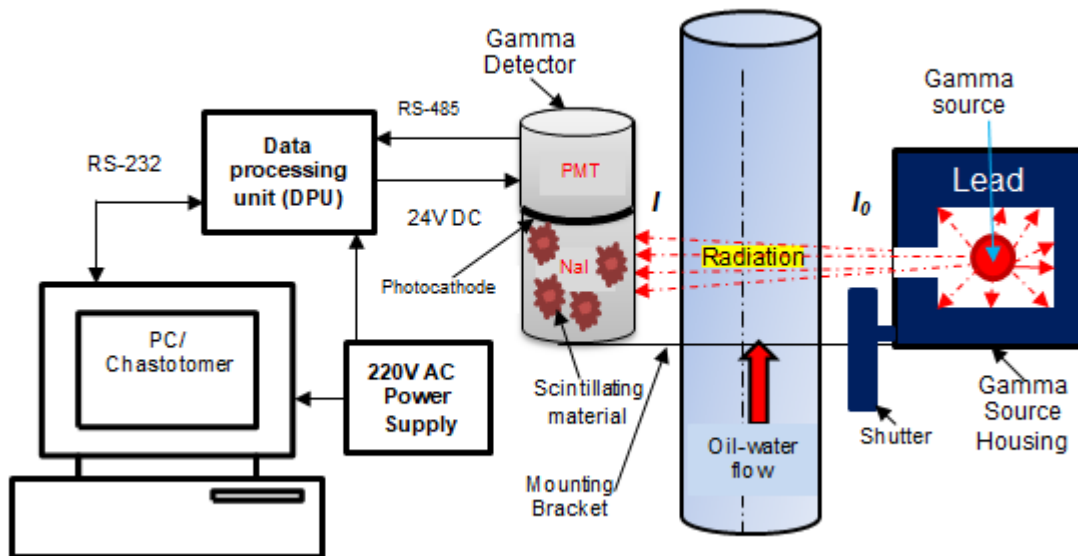
601

602 **Figure 3-6** Example of the continuous wave ultrasound signal and its: (a) Raw signal,
 603 and (b) STFT, for conditions: $V_m = 1.25$ m/s, $WC = 60\%$, and a 10-kHz signal
 604 acquisition frequency.

605 **3.4 Gamma densitometer system**

606 The gamma densitometer used in this study employs Caesium-137 isotope. The gamma
 607 source, detector and a data processing unit are manufactured by the Neftemer® Ltd as a
 608 clamp-on multiphase flowmeter. The gamma source housing provides an outlet that
 609 produces a cone of beam six degree wide having uniform physical properties directed
 610 across the pipe diameter. The caesium-137 isotope emits 0.1 – 0.94 MeV photon
 611 energies. The detector unit comprises scintillation crystals (NaI), photomultiplier tube
 612 (PMT), amplifier electronics and single channel analyser (SCA) and a temperature
 613 control. The PMT contains photocathode and focussing electrodes. The scintillation
 614 crystals produce a pulse of visible light with energy proportional to that of the incident
 615 gamma photon and are detected by the photocathode which produces electrons by
 616 photoelectric effect. The amount of the electrons by the photocathode is low and it has
 617 to be amplified by the photomultiplier which converts the light pulses into voltage
 618 pulses of proportional amplitudes. The voltage pulses undergo signal conditioning then

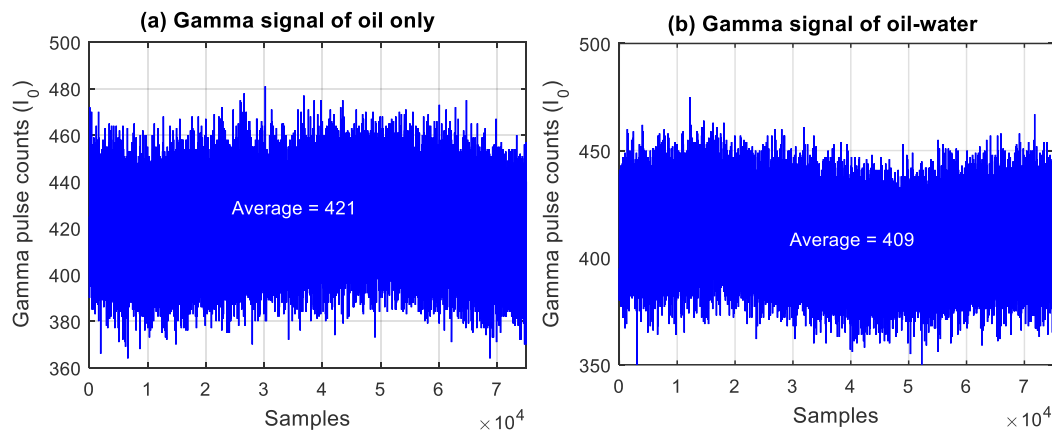
619 passed on to channel analysers for classification(Kumara et al., 2010a; Tesi, 2011).The
 620 scattering of the gamma electromagnetic radiation by the matter via interaction of the
 621 photons with the matter can take several forms but the two methods of photoelectric or
 622 Compton scattering are the most frequency used at low energy emissions (Kumara et
 623 al., 2010a). The photoelectric type is the one used in the present study.
 624 The gamma-source and detector are arranged diametrically opposite to each other with
 625 the gamma densitometer source emitting a narrow beam of radiation and an opposing
 626 detector scan across the pipe-section for measuring the average flow volume fraction
 627 across the whole pipe diameter(Kumara et al., 2010a). Figure 3-7 shows the schematic
 628 diagram of the gamma densitometer instrumentation set up in which the variables I_0
 629 and I are the incident and the received intensities of the gamma-rays.



630
 631 **Figure 3-7** Schematic diagram of a single-beam gamma densitometer system
 632 Single phase flow calibration is required for the determination of the volume fractions at
 633 the beginning of every test point (Falcone et al., 2009). Therefore, the gamma count
 634 rates of single phase water flow I_w and of oil flow I_o were obtained and recorded. The

635 data is collected every test point and then stored for further processing. The flow
636 parameters such as phase fraction and the mixture density can be calculated from the
637 average pulse count rate and the calibration results (Falcone et al., 2009; Kumara et al.,
638 2010a)

639 Figure 3-8 shows Examples of the gamma densitometer counts from (a) oil only signal,
640 and (b) oil-water signal, for conditions overall velocity $V_m = 1.25$ m/s, WC =60%. A
641 sampling at 250 Hz frequency was used and a total of 75,000 samples (which
642 corresponds to 300 s sampling time (5 minutes) were collected at each sampling point.

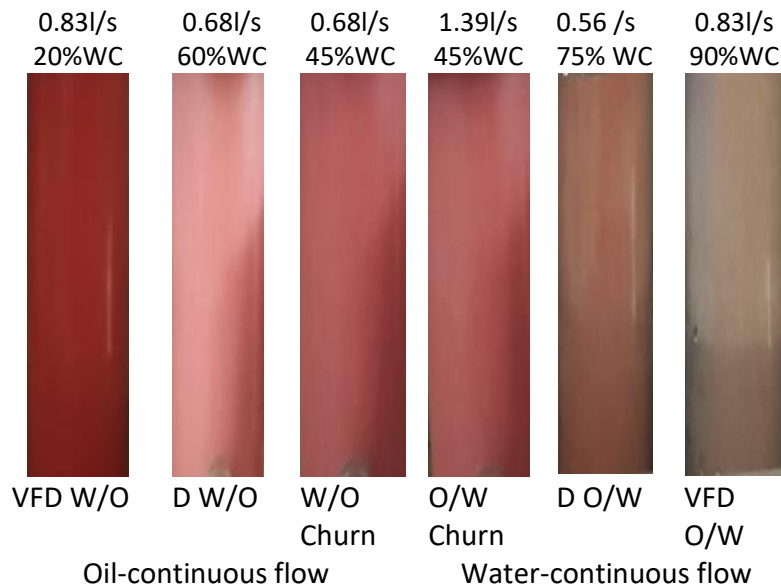


643

644 **Figure 3-9** Gamma-ray densitometer pulse counts obtained from (a) Oil only signal,
645 and ((b) oil-water signal

646 **3.5 Experimental observation**

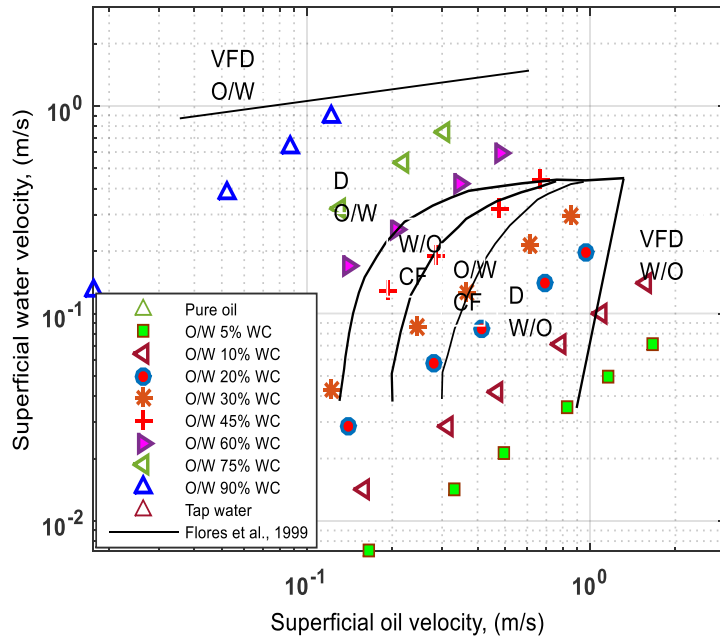
647 From the observation of these experiments, vertical upwards oil/water flows, it was
648 evident that when the flow velocities were relatively high (e.g. the mixture velocity
649 above 0.60 m/s), the oil and water were well mixed and the flow regime was a dispersed
650 flow. When the mixture velocity was low, then the flow regime was churn flow. This
651 observation is also consistent with the recommended criteria for discriminating
652 dispersed and non-dispersed oil/water upwards flows by API, (2015). More detailed
653 flow regime classifications were reported by other published studies.



654

655 **Figure 3-10** Photos of the flow pictures taken in the experiments

656 Flores et al., (1999) conducted experimental investigation for characterization of
 657 vertical oil-water flow and defined the flow patterns in oil-water two-phase vertical flow
 658 into six flow patterns belonging to two dominant classes: *oil-continuous flow* (water in
 659 oil churn flow, dispersion water in oil, and very fine dispersion water in oil), and *water-*
 660 *continuous flow* (oil in water churn flow, dispersion oil in water, and very fine
 661 dispersion oil in water). in the present study, the oil-water upward vertical flow map
 662 produced by Flores et al. (1999) was used to map the flow data as shown in Figure
 663 3-11. Furthermore, we developed the flow measurement model that allows study of the
 664 oil-water two-phase flow based on (1) the oil continuous flow, flow and (2) the water
 665 continuous flow, and to predict the superficial flow velocity of the oil and water by
 666 using established drift-flux model. These two main flow patterns were expected to occur
 667 in oil-water two-phase flow according to some authors (Dong et al., 2016, 2015; Lovick
 668 and Angeli, 2004).



669

670 **Figure 3-11** the experimental test points plotted on the transition map by Flores et al.,
 671 (Flores et al., 1999)

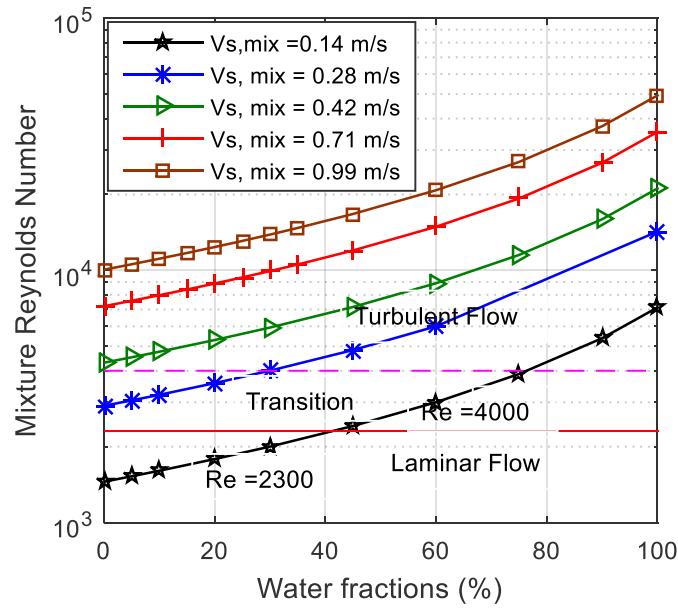
672 **3.6 Reynolds number of the oil-water two-phase flow**

673 The Reynolds number (Re), is the ratio of inertial forces to viscous forces acting on a
 674 fluid. For a circular pipe is laminar for $Re \leq 2300$, turbulent for $Re \geq 4000$, and in
 675 between them is transitional. Reynolds number of the oil-water two-phase flow
 676 investigated in the present study was plotted against the input flow volume water
 677 fraction. Figure 3-12 shows a plot of Reynolds number of the oil-water two-phase
 678 mixture flow velocity range from 0.14 m/s to 1 m/s and the input water cut from 0% to
 679 100%. The plot is used for classification of the flow velocity profiles. The Reynolds
 680 number Re for two-phase flow is defined as:

$$Re = \frac{\text{Inertial forces}}{\text{Viscous forces}} = \frac{\rho_m V_m D}{\mu_m} \quad (3-1)$$

681 where μ_m is the dynamic viscosity of the two-phase flow and V_m is the mixture flow
 682 velocity.

683



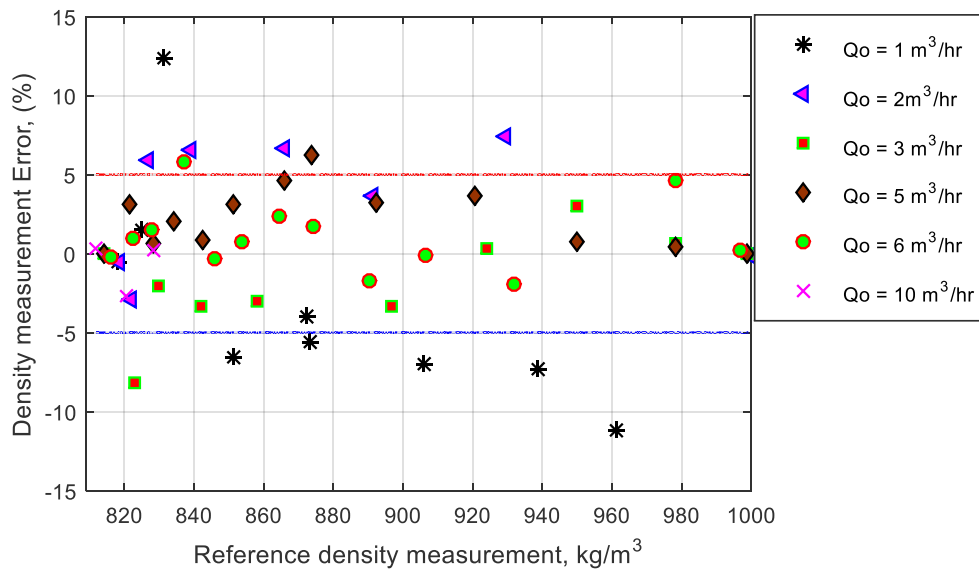
684

685 **Figure 3-12** Mixture flow Reynolds number as function of water fraction

686 4 Results and discussion

687 4.1 Mixture density measurement

688 Using the non-invasive capability of the gamma-ray densitometer, the density of the
689 mixture flow and the oil volume fraction investigated in these experiments were
690 measured. Figure 4-1 shows mixture densities obtained from the measurements with
691 gamma-ray densitometer compared with the reference Coriolis flowmeter. From the
692 Figure 4-1, it can be seen that the difference between the densitometer measurements
693 and the reference mixture density rose up to $\pm 13\%$ at $1\text{m}^3/\text{hr}$ and then fell down to
694 less than $\pm 5\%$ at $6\text{m}^3/\text{hr}$. So, in oil-water two phase flows, the measurement of the
695 mixture flow density is affected by the flow rate.



696

697 **Figure 4-1** The relative errors of the mixture flow density

698 **4.2 Mixture flow velocity measurement.**

699 The oil-water two-phase flow is considered as a water-continuous flow when the inlet
700 water-cut is greater than or equal to 30%. Otherwise, it is considered as an oil-
701 continuous flow(Brauner and Ullmann, 2002; Dong et al., 2016). The mixture mean
702 flow velocities were computed from the measured local velocities in the measuring
703 volume and the flow velocity profile models through the applying equations (2-16) and
704 (2-29). The results are shown in Figure 4-2 and Figure 4-3 for the oil-continuous flow
705 and for water-continuous flow respectively.

706 The relative error and the absolute error for the flow measurement results are calculated
707 using (4-1)and (4-2) respectively.

$$E_r = \frac{Data_{est} - Data_{ref}}{Data_{ref}} \times 100\% \quad (4-1)$$

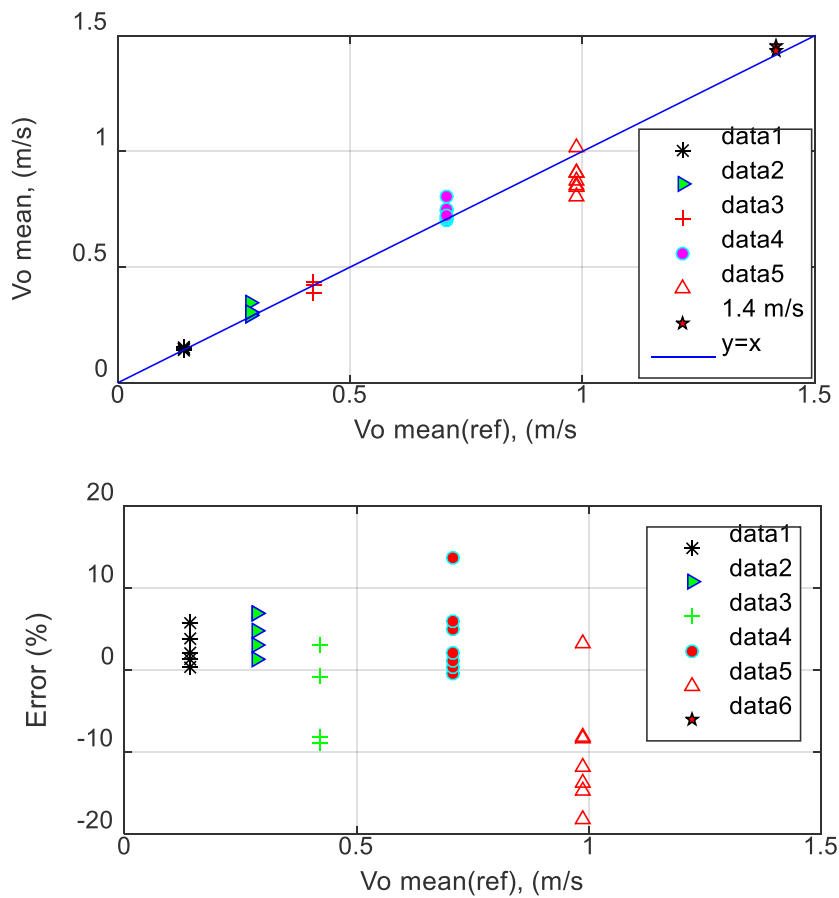
708 where $Data_{est}$ is the estimated result in oilr-continuous flow (V_{o-m}) and water-
709 continuous flow(V_{w-m})and $Data_{ref}$ is the reference mixture flow rate measured by the
710 single phase flowmeters. The average absolute of the error is:

$$\epsilon_{ave} = 1/N_s \sum |E_r| \quad (4-2)$$

711 where N_s is the sample number.

712 4.2.1 Oil-continuous flow

713 Comparison between the estimated mixture flow velocity predicted by equation (2-16)
 714 and the total mixture flow velocity obtained by the flow rates at the inlets is presented in
 715 Figure 4-2. For evaluating the accuracy of the proposed model, calculated both the
 716 relative error and the absolute error of the results. It can be seen that at most test points,
 717 the relative error (E_r) is within $\pm 8.0\%$ of the reference mixture flow velocity. This
 718 agreement is considered quite good considering the statistical nature of the experiments
 719 and the oil-water flow phenomena.



720

721 **Figure 4-2** Measurement mean velocity of oil-continuous flow in oil-water two-phase
722 flow

723 Finally, the mixture superficial velocity of oil-continuous flow was predicted by the
724 equation (2-16) and the results show that the mean relative error was equal to 5.2% and
725 maximum relative error was equal to 17.6%.

726 **4.2.2 Water-continuous flow**

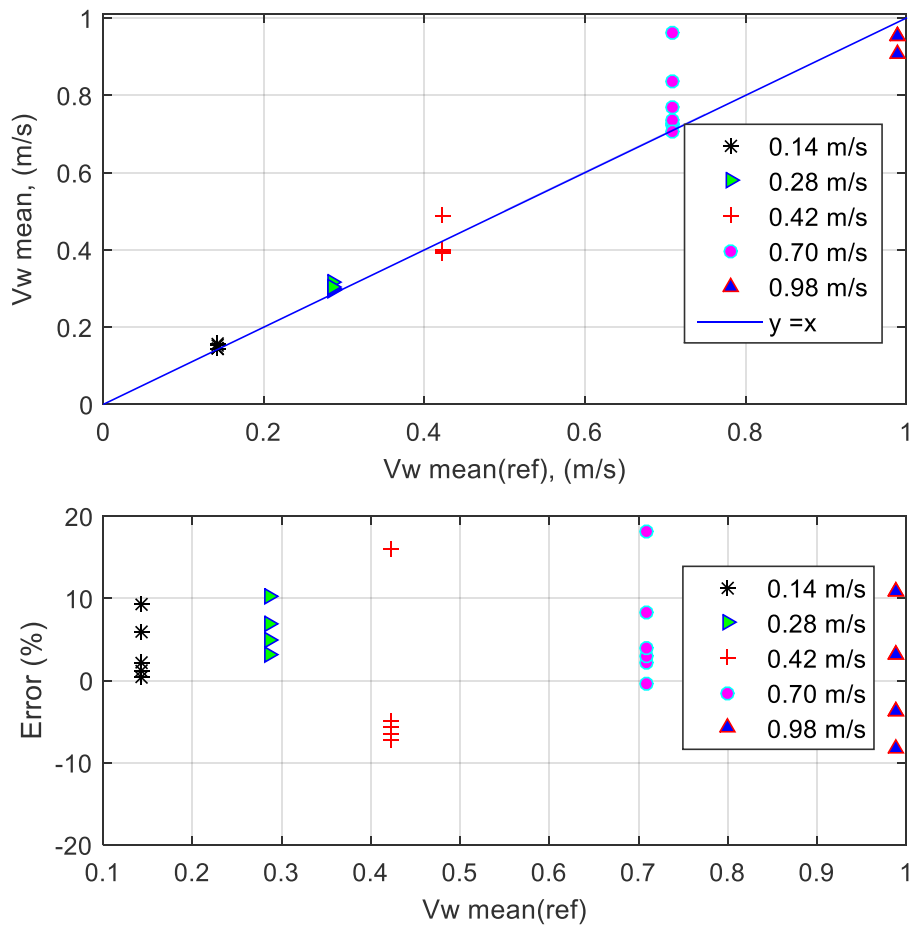
727 The mean superficial velocity of the water-continuous flow can be estimated using the
728 measured flow velocity in the measuring volume and corrections to account velocity
729 profile in the pipe. The water-continuous in the present experimental set-up can be
730 estimated using equation (2-29). The results for the water-continuous flow model were
731 similar to the oil-continuous flow model. Figure 4-3 show the results from the water-
732 continuous flow model.

733 For the Eqn.(2-29), the friction factor's coefficient b and exponent n are to be
734 determined for estimating the mixture flow velocity. There are many experimental data
735 for these two coefficients in the literature. For an example, Blasius correlation for a tube
736 with a smooth wall and for $2000 < Re < 10^5$ set the values of the coefficient b and
737 exponent n as 0.316 and 0.25 (Descamps et al., 2006). In addition, the values of the
738 coefficients b and n presented by Bannwart (Bannwart, 2001) for the Reynolds number
739 range of the 2×10^3 to 10^5 range between 0.19 to 0.443 and 0.19 to 0.28 respectively.
740 In the present experiment, selection of the coefficient b and exponent n were obtained
741 by using the Blasius correlation as a benchmark and then the flow velocity predictions
742 were turned to best fit fit for each flow velocity. the Blasius correlation($b = 0.316$ and
743 exponent $n = 0.25$) equivalent values in the present study are as shown in Table 4.

744 **Table 4** Friction factor coefficients

Mixture flow velocity, m/s Present experiment predicted values of
 coefficient b and exponent n

1.	0.143	$b = 8.0;$	$n = 0.008$
2.	0.285	$b = 4;$	$n = 0.06$
3.	0.423	$b = 2;$	$n = 0.07$
4.	0.708	$b = 0.80;$	$n = 0.06$
5.	0.988	$b = 0.316;$	$n = 0.025$



745

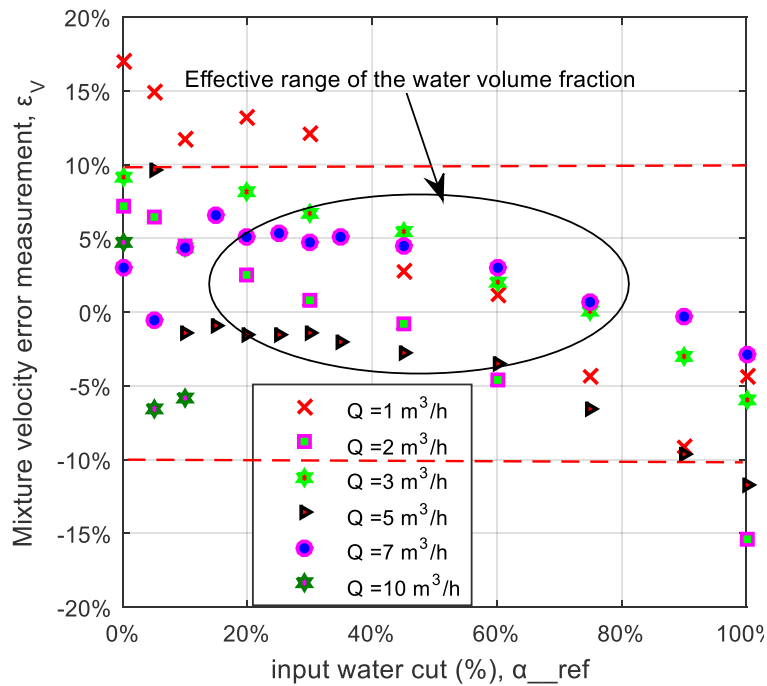
746 **Figure 4-3** Measurement mean velocity of water-continuous flow in oil-water two-
 747 phase flow

748 As illustrated in Figure 4-3, the mixture flow velocities estimated when the flow
749 condition is water-continuous flow-mean relative error was equal to 2.8% and
750 maximum relative error was equal to 17%.

751 Moreover, in comparison with the horizontal oil-water two-phase measurement using
752 CWDU flow sensor method by (Dong et al., 2015) with the present experiment, the
753 mixture flow velocity estimated in water-continuous flow maximum relative error was
754 equal to 11.8% and mean error 3.11% while the oil-continuous flow conditions has
755 maximum relative error 12.2% and mean relative error 4.8% respectively. This
756 suggests that the present study conducted on a vertical flow pipe good non-invasive
757 flow measurement system can readily be achieved with using the ultrasound Doppler
758 method.

759 **4.3 Effect of water-cut on mixture flow velocity**

760 The mixture velocities are evaluated for various input water-cut and these
761 measurements result are then compared to the reference to experimental results. Figure
762 shows that 87% points measured values are well within $\pm 10\%$ and 56% points are
763 within $\pm 5\%$. The errors in the measured mixture flow densities for the different
764 volume fraction were was due to the flow structure changes even at constant the total
765 mixture flow rate.



766

767 **Figure 4-4** Measured mixture flow velocity in varied water volume fractions

768 **4.4 Prediction of the superficial velocities of the oil and the water**

769 The oil-water mixture flow velocity in both oil-continuous flow and water-continuous
 770 flow can be determined using the CWDU method proposed in this study. However, the
 771 superficial velocities of the oil and the water are frequently required to be
 772 determined(Lucas and Jin, 2001). The individual phase superficial velocities of oil and
 773 of water were estimated using the drift-flux model in which the mixture flow velocity
 774 and phase fraction are the inputs. The results were compared with single phase
 775 flowmeter measurement at the flow inlets prior to the mixing.

776 Equations (2-34) and (2-35) were used for the calculation of superficial flow velocity of
 777 oil and of water respectively and the initial results showed slight underestimation and
 778 overestimation. Hence, correction factors are essential to modify both Eqns.(2-34) and
 779 (2-35). Since the original results obtained from using the equations (2-34) and
 780 (2-35)were linear, consequently, the two equations were corrected individually using

781 determined by using a least-squares method based on linear portions of the original
 782 estimates. These yielded the equations which resulted in in Eqns. (4-3) and (4-4) for the
 783 superficial flow velocity of oil and water respectively, as:

$$V_{so-mean} = 0.78 * V_{so} \quad (4-3)$$

784 and

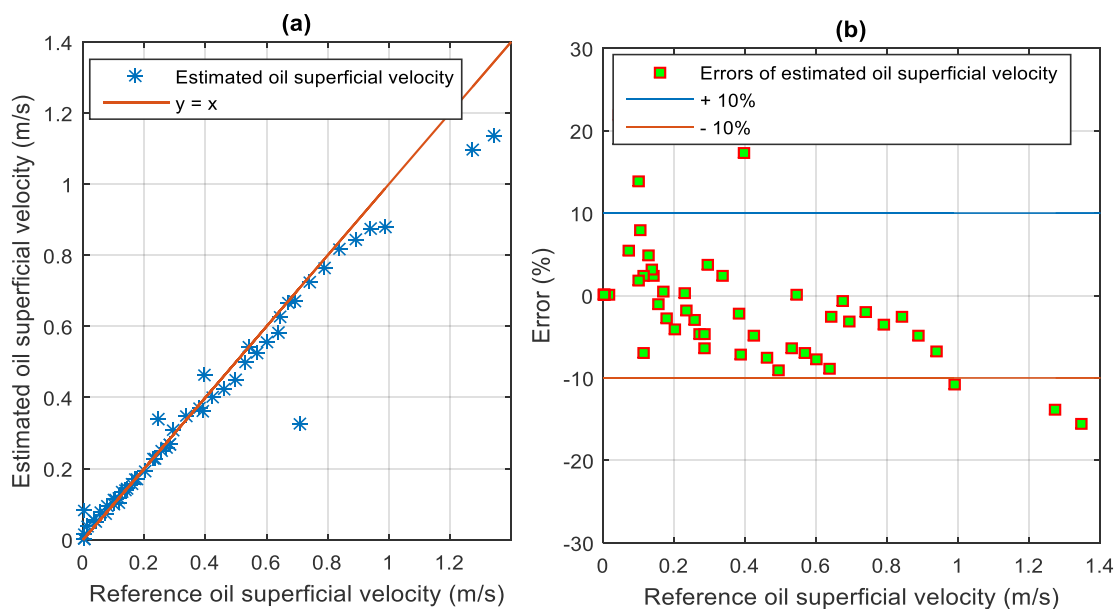
$$V_{sw-mean} = 1.08 * V_{sw} \quad (4-4)$$

785 Figure 4-5 shows the results for estimation of superficial velocity of oil using the
 786 equation (4-3). Similarly, Figure 4-6 shows the results of using Eqn. (4-4) for water
 787 superficial flow velocity respectively. The superficial phase flow velocity of oil is V_{soi} ,
 788 and $V_{R,soi}$ as the reference value. The relative error δ_i is defined as:

$$\delta_i = \frac{V_{soi} - V_{R,soi}}{V_{R,soi}} \times 100\% \quad (4-5)$$

789 where i is the test point number, and the average relative error can be expressed as:

$$\overline{\delta}_{V_{so}} = \frac{1}{N} \sum_{i=1}^N |\delta_i| \quad (4-6)$$

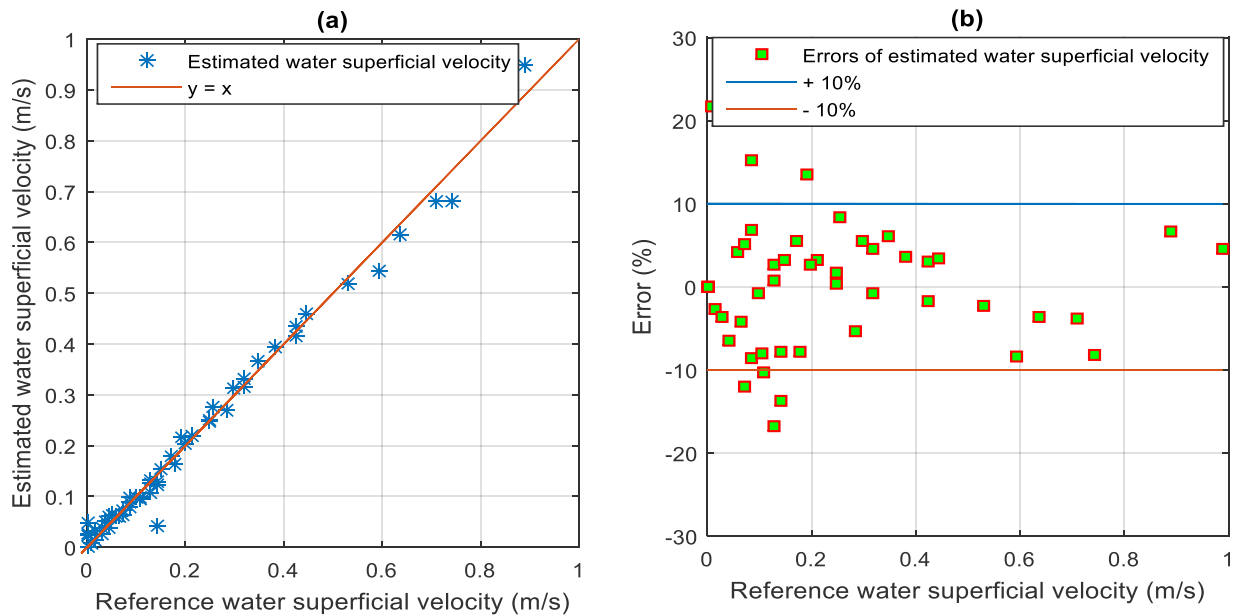


790

791 **Figure 4-5** (a) the predicted superficial velocity of oil by equation (4-3) versus the
 792 reference superficial velocity of oil (b) The percentage error in superficial velocity of oil
 793 versus the reference superficial velocity of oil

794 Figure 4-5 illustrates the comparison of the estimated superficial flow velocity of oil
 795 obtained from equation (4-3) plotted against the reference oil superficial velocity. It was
 796 observed that the average relative error $\delta_{V_{so}}$ was equal to 4.5% and the maximum
 797 relative error was equal to 19.15%.

798 Using two equations similar to equations (4-5) and (4-6) the percentage error in the
 799 predicted water superficial velocity V_{sw} be calculated for each test point. Figure 4-6
 800 illustrates the comparison of the estimated water phase flow velocity obtained from
 801 equation (4-4) plotted against the reference water superficial velocity. Again, it was also
 802 observed that the average relative error $\delta_{V_{so}}$ was equal to 5.98% and the maximum
 803 relative error was equal to 25.58%



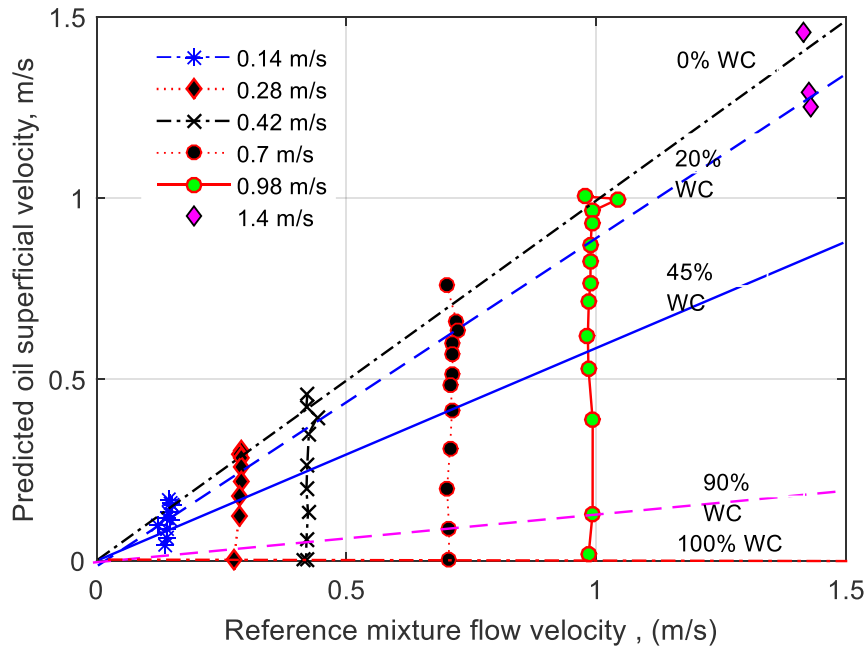
804

805 **Figure 4-6** (a) the predicted superficial velocity of water by equation (4-4) versus the
806 reference superficial velocity of water (b) the percentage error in superficial velocity of
807 water versus the reference superficial velocity of water

808 The overall accuracy on the superficial phase velocities estimated have average relative
809 errors of around 4.5% for oil flow velocity, and 5.9% for water flow velocity.
810 However, the error of superficial oil flow velocity estimation rose when the water-cut
811 increased at the initial stages but the relative error decreased as the water cut increased
812 up further. These suggest that that smaller fraction of oil enlarges the relative error at
813 the lower water-cut but relative error fell below 10% at the higher water-cut. The error
814 of superficial water flow velocity was also rose at the lower water-cut but decreased
815 when water-cut increases, the error of superficial water flow velocity predictions was
816 much higher at low water-cut. This phenomenon suggests that the input water-cut range
817 affects the prediction accuracy of both superficial flow velocities. Analyses on effect of
818 water-cut on superficial phase flow velocities estimation is provided in section 4.6.

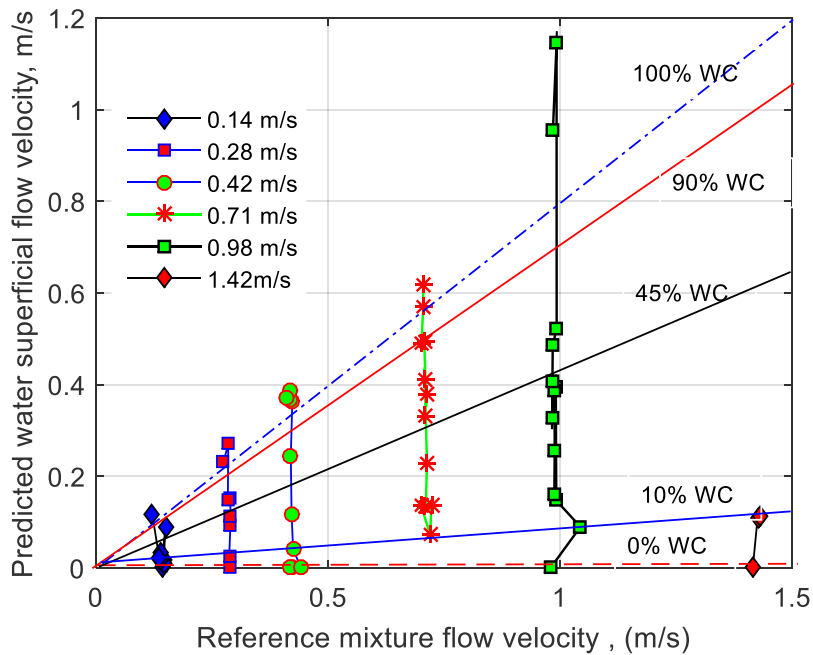
819 **4.5 Superficial velocity of oil and water versus mixture flow velocity**

820 Predicted superficial velocity of oil and of water are reported in Figure 4-5 and Figure
821 4-6 respectively. Here predicted superficial velocities of oil and of water are reported as
822 a function of the reference mixture flow velocity in Figure 4-7 and Figure 4-8. From the
823 plots, it is evident that oil superficial velocity basically fits the mixture flow velocity
824 data, especially between the water-cut range of 20% and 90%. These translate to a good
825 agreement between Predicted superficial velocity of oil and the oil flow velocity
826 measured with the reference flowmeter in the range tested. A Similar trend was also
827 observed in the comparison of the water superficial velocity and mixture flow velocity
828 measured by the reference flowmeter.



829

830 **Figure 4-7** predicted oil superficial flow velocity versus reference mixture flow velocity



831

832 **Figure 4-8** predicted water superficial flow velocity versus reference mixture flow
833 velocity

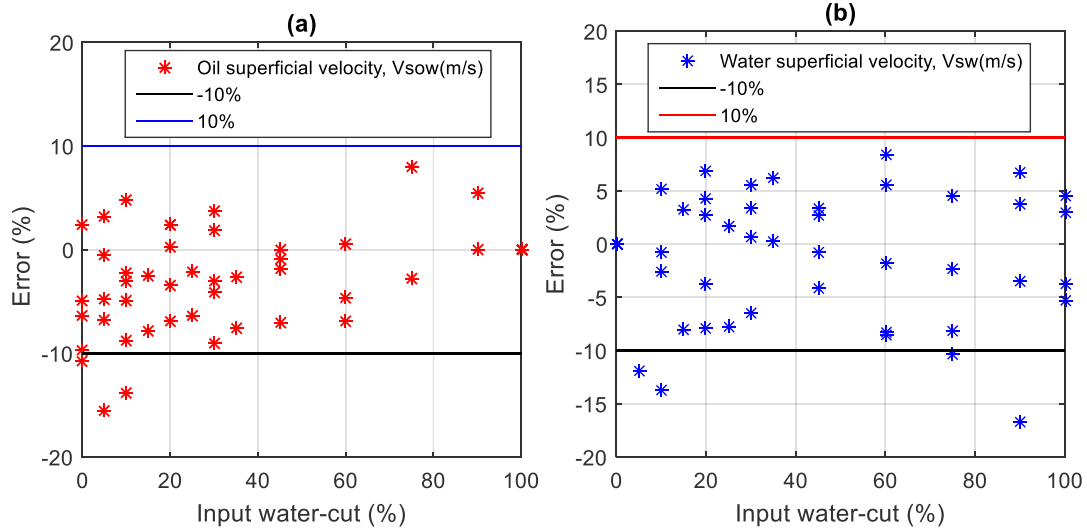
834 Figure 4-7 and Figure 4-8 show that prediction of the superficial velocities of oil and water
835 using the drift-flux model has been validated by the results of the reference single phase

836 flowmeters. It is clear from Figure 4-7 that the superficial velocity of oil are in accordance with
837 the mixture flow velocity when the oil flow is the continuous, but deviated slightly from the
838 mixture flow velocity as the water-cut increased further. The distribution of the water superficial
839 velocity, however, showed opposite trend. These are slight deviations from the mixture flow
840 velocity are as a result variation in the flow velocity profiles. Oil-water two-phase flow
841 measurement using the CWDU sensor in a vertical pipe has not been reported in the literature.

842 **4.6 Effect of water-cut on superficial phase flow velocities**

843 It is important to note that in this study, both flow rates and water-cuts were varied in
844 order to evaluate meter performance under varying flow conditions. The influence of
845 the water volume fraction data were evaluated based on the errors calculated in the
846 results of both superficial velocities of oil flow and water flow. The errors are the
847 difference between the single phase flow measured at the inlet and results obtained from
848 the proposed method. The phase superficial velocities dependent on both the in situ
849 holdup and the mixture flow velocity. The variation of relative error (ϵ) of mean oil
850 superficial flow velocity and mean water superficial flow velocity (expressed in per cent
851 of deviation from the inlet measurement) versus water-cut at the inlet are shown in
852 Figure 4-9 (a) and (b).

853



854

855 **Figure 4-9** Relative error (ϵ) of mean in phase superficial flow velocities

856 ($V_{so-mean}$ and $V_{sw-mean}$) versus input water-cut

857 However, experimental results in an inclined pipe by (Lucas and Jin, 2001) who
 858 predicted the superficial velocities of oil and water by using a differential pressure
 859 measurement and drift-flux model, showed markedly scatter in the data due to variation
 860 in the water-cut. But the effect of water-cut variation on the phase flow velocity is not
 861 so large within the present experimental condition.

862 It is interesting to note, the errors encountered in the measurement of water phase flow
 863 velocity were at low total flow rate and low water-cut. However, increasing the total
 864 flow rate reduces the water phase measurement errors. While the errors encountered in
 865 the measurement of the oil phase flow were very high at both very low water-cut
 866 (<20%) and very high water-cut (>80%). It was concluded that these trends in the errors
 867 were due to increased turbulence in the pipe. Turbulent flow generates random radial
 868 movement of the droplets therefore it is a contributory factor in the inaccuracy of the
 869 measurement.

870 **5 Conclusions**

871 This paper presents a method for measuring the mixture and individual phase velocities
872 in oil-water two-phase vertical pipe flows using a continuous wave Doppler ultrasonic
873 (CWDU) flow sensor, a gamma densitometer and theoretical correlations based on
874 velocity profiles and the drift-flux model. It was verified and assessed in both the water-
875 continuous flows and oil-continuous flows in a near-industrial scale test rig with the use
876 of industry standard single phase flow meters as references. Errors between the
877 measured oil and water phase flow velocities and those of the respective flow meters are
878 calculated in terms of mean relative error and maximum relative error between the test
879 flowmeters and the reference flowmeters.

880 The velocity of sound in oil and in water is different. Therefore, we adopted a hybrid
881 method of estimating the sound velocity of the mixture flow which encompasses the
882 contributions of the phase fractions based on the homogenous flow model. The sound
883 speed of the oil-water mixture flow play is vital to the ultrasonic Doppler technique in
884 the flow velocity measurement.

885 The differences between flow rates obtained from the proposed method and the
886 reference single phase flowmeters depend on the total flow rate as well as the water-cut.

887 The maximum relative differences were found at the low end of the flow rates. The
888 values of the oil-water two-phase flow such as the mixture density, sound speed, and
889 viscosity are estimated based on the homogeneous flow model to simplify the
890 calculation of the theoretical models. These models depend on phase volume fraction
891 estimation. Therefore, the calibration of the gamma densitometer has to be made very
892 accurately or else the estimated flow rates can have significant errors.

893 In general this oil-water two-phase flow measurement technique developed has effective
894 range when the water volume fraction was between 25% and 75%. This proposed
895 system is entirely non-invasive without utilising any electrical conductance sensor as in
896 in the previous studies(Faraj et al., 2015; Jin et al., 2020; Tan et al., 2016). Therefore, it
897 could be implemented in the pipeline without breaking in the pipeline. Further studies
898 are recommended to focus on experimental investigations using crude oil (instead of
899 mineral) and saline water (instead of tap water) to simulate more practical field
900 conditions of the oil water flows in production operations.

901 **6 References**

- 902 Abbagoni, B.M., Yeung, H., 2016. Non-invasive classification of gas-liquid two-phase
903 horizontal flow regimes using an ultrasonic Doppler sensor and a neural network.
904 Meas. Sci. Technol. 27. <https://doi.org/10.1088/0957-0233/27/8/084002>
- 905 API, M., 2015. Chapter 8.2- Manual Sampling of Petroleum and Petroleum Products,
906 in: API Manual of Petroleum Measurement Standards Standard Practice for
907 Automatic Sampling of Petroleum and Petroleum Products. API Publishing
908 services, Washington D.C, United State.
- 909 Baker, D.W., Yates, G.W., 1973. Technique for studying the sample volume of
910 ultrasonic Doppler devices. Med. Biol. Eng. 766–770.
- 911 Bannwart, A.C., 2001. Modeling aspects of oil – water core – annular flows. J. Pet. Sci.
912 Eng. 32, 127–143.
- 913 Brauner, N., 2002. Liquid-Liquid Two-Phase Flow Systems, in: Bertola, V. (Ed.),
914 Udine, Italy, pp. 1–59.
- 915 Brauner, N., Ullmann, A., 2002. Modeling of phase inversion phenomenon in two-
916 phase pipe flows. Int. J. Multiph. Flow 28, 1177–1204.

917 Brody, W.R., Meindl, J.D., James, D., 1974. Theoretical analysis of the CW doppler
918 ultrasonic flowmeter. *IEEE Trans. Biomed. Eng.* 21, 183–192.
919 <https://doi.org/10.1109/TBME.1974.324381>

920 Case, M., Micheli, M., Arroyo, D., Hillard, J., Kocanda, M., 2013. Ultrasonic blood
921 flow sensing using doppler velocimetry. *Int. J. smart Sens. Intell. Syst.* 6, 1298–
922 1316.

923 Çengel, Y.A., 2007. Flow in pipes, in: *Heat and Mass Transfer: A Practical Approach*.
924 McGraw-Hill, Pennsylvania State University, pp. 321–343.

925 Chaudhuri, A., Sinha, D.N., Zalte, A., Pereyra, E., Webb, C., Gonzalez, M.E., 2014.
926 Mass fraction measurements in controlled oil-water flows using noninvasive
927 ultrasonic sensors. *J. Fluids Eng.* 136, 1–8. <https://doi.org/10.1115/1.4026055>

928 Chemlou, N.S., Chaib, K., Mostefa, K., 2009. Simultaneous measurements of the solid
929 particles velocity and concentration profiles in two phase flow by pulsed ultrasonic
930 Doppler velocimetry. *J. Braz. Soc. Mech. Sci. Eng.* XXXI, 333–343.

931 Chen, J., Xu, L., Cao, Z., Zhang, W., Liu, X., 2015. Water cut measurement of oil –
932 water flow in vertical well by combining total flow rate and the response of a
933 conductance probe. *Meas. Sci. Technol.* 10pp. [https://doi.org/10.1088/0957-](https://doi.org/10.1088/0957-0233/26/9/095306)
934 [0233/26/9/095306](https://doi.org/10.1088/0957-0233/26/9/095306)

935 Da, N., Sirivat, A., Siemanond, K., Wilkes, J.O., 2007. Vertical two-phase flow regimes
936 and pressure gradients : Effect of viscosity. *Exp. Therm. Fluid Sci.* 31, 567–577.
937 <https://doi.org/10.1016/j.expthermflusci.2006.03.030>

938 Descamps, M., Oliemans, R.V.A., Ooms, G., Mudde, R.F., Kusters, R., 2006. Influence
939 of gas injection on phase inversion in an oil – water flow through a vertical tube.
940 *Int. J. Multiph. Flow* 32, 311–322.

941 <https://doi.org/10.1016/j.ijmultiphaseflow.2005.10.006>

942 Dong, X., Tan, C., Yuan, Y., Dong, F., 2016. Measuring oil – water two-phase flow
943 velocity with continuous-wave ultrasound Doppler sensor and drift-flux model.
944 IEEE Trans. Instrum. Meas. 65, 1–10.

945 Dong, X., Tan, C., Yuan, Y., Dong, F., 2015. Oil – water two-phase flow velocity
946 measurement with continuous wave ultrasound Doppler. Chem. Eng. Sci. 135,
947 155–165. <https://doi.org/10.1016/j.ces.2015.05.011>

948 Du, M., Jin, N., Gao, Z., Wang, Z., Zhai, L., 2012. Flow pattern and water holdup
949 measurements of vertical upward oil – water two-phase flow in small diameter
950 pipes. Int. J. Multiph. Flow 41, 91–105.
951 <https://doi.org/10.1016/j.ijmultiphaseflow.2012.01.007>

952 Eskin, D., Taylor, S., Mark, S., Abdallah, W., 2017. Modeling droplet dispersion in a
953 vertical turbulent tubing flow. Chem. Eng. Sci. 173, 12–20.
954 <https://doi.org/10.1016/j.ces.2017.07.023>

955 Falcone, G., Hewitt, G.F., Alimonti, C., 2009. Multiphase flow metering: principles and
956 applications, First edit. ed. Elsevier Science, Oxford, United Kingdom.

957 Faraj, Y., Wang, M., Jia, J., Wang, Q., Xie, C., Oddie, G., Primrose, K., Qiu, C., 2015.
958 Measurement of vertical oil-in-water two-phase flow using dual-modality ERT –
959 EMF system. Flow Meas. Instrum. 46, 255–261.
960 <https://doi.org/10.1016/j.flowmeasinst.2015.08.010>

961 Figueiredo, M.M.F., Goncalves, J.L., Nakashima, A.M. V, Fileti, A.M.F., Carvalho,
962 R.D.M., 2016. The use of an ultrasonic technique and neural networks for
963 identification of the flow pattern and measurement of the gas volume fraction in
964 multiphase flows. Exp. Therm. Fluid Sci. 70, 29–50.

965 <https://doi.org/10.1016/j.expthermflusci.2015.08.010>

966 Flores, J., Chen, X., Sarica, C., Brill, J., 1999. Characterization of oil–water flow
967 patterns in vertical and deviated wells, in: SPE Annual Technical Conference and
968 Exhibition. SPE, San Antonio, Texas, pp. 5–8. <https://doi.org/10.2118/56108-PA>

969 Flores, J.G., Sarica, C., Chen, T.X., Brill, J.P., 1998. Investigation of holdup and
970 pressure drop behavior for oil-water flow in vertical and deviated wells. *J. Energy*
971 *Resour. Technol.* 120, 8–14.

972 Garcia-Lopez, A., Sinha, D.N., 2008. Enhanced acoustic separation of oil-water
973 emulsion in resonant cavities. *Open Acoust. J.* 1, 66–71.

974 Grassi, B., Strazza, D., Poesio, P., 2008. Experimental validation of theoretical models
975 in two-phase high-viscosity ratio liquid – liquid flows in horizontal and slightly
976 inclined pipes. *Int. J. Multiph. Flow* 34, 950–965.
977 <https://doi.org/10.1016/j.ijmultiphaseflow.2008.03.006>

978 Harmathy, T.Z., 1960. Velocity of Large Drops and Bubbles in Media of Infinite or
979 Restricted Extent. *Am. Inst. Chem. Eng. J.*

980 Hasan, A.R., Kabir, C.S., 1998. A simplified model for oil-water flow in vertical and
981 deviated wellbores, in: SPE Annual Technical Conference and Exhibition. New
982 Orleans, Louisiana,.

983 Hu, B., Matar, O.K., Hewitt, G.F., Angeli, P., 2007. Mean and turbulent fluctuating
984 velocities in oil – water vertical dispersed flows. *Chem. Eng. Sci.* 62, 1199–1214.
985 <https://doi.org/10.1016/j.ces.2006.10.008>

986 Huang, S., Xie, C., Lenn, C., Yang, W., Wu, Z., 2013. Issues of a combination of
987 ultrasonic Doppler velocity measurement with a venturi for multiphase flow
988 metering, in: The SPE Middle East Oil and Gas Show and Conference Held.

- 989 Society of Petroleum Engineers, Manama, pp. 1–9.
- 990 Ibarra, R., Zadrazil, I., Matar, O.K., Markides, C.N., 2017. Dynamics of liquid-liquid
991 flows in horizontal pipes using simultaneous two-line planar laser-induced
992 fluorescence and particle velocimetry. *Int. J. Multiph. Flow.*
993 <https://doi.org/10.1016/j.ijmultiphaseflow.2017.12.018>
- 994 Ismail, I., Gamio, J.C., Bukhari, S.F.A., Yang, W.Q., 2005. Tomography for multi-
995 phase flow measurement in the oil industry. *Flow Meas. Instrum.* 16, 145–155.
996 <https://doi.org/10.1016/j.flowmeasinst.2005.02.017>
- 997 Jana, A.K., Das, G., Das, P.K., 2006. Flow regime identification of two-phase liquid –
998 liquid upflow through vertical pipe. *Chem. Eng. Sci.* 61, 1500–1515.
999 <https://doi.org/10.1016/j.ces.2005.09.001>
- 1000 Jin, N., Yu, C., Han, Y., Yang, Q., Ren, Y., Zhai, L., 2020. The performance
1001 characteristics of electromagnetic flowmeter in vertical low-velocity oil-water two-
1002 phase flow. *IEEE sensors* 21, 464–475.
1003 <https://doi.org/10.1109/JSEN.2020.3013327>
- 1004 Kikura, H., Yamanaka, G., Aritomi, M., 2004. Effect of measurement volume size on
1005 turbulent flow measurement using ultrasonic Doppler method. *Exp. Fluids* 36,
1006 187–196. <https://doi.org/10.1007/s00348-003-0694-x>
- 1007 Kouame, D., Girault, J., Remenieras, J., Chemla, J.-P., Marc, L., 2003. High resolution
1008 processing techniques for ultrasound Doppler velocimetry in the presence of
1009 colored noise . Part II: multiple phase pipe-flow velocity measurement. *IEEE*
1010 *Trans. Ultrason. Ferroelectr. Freq. Control* 50.
- 1011 Kudela, H., 2010. Turbulent flow, in: Pdf Document. available at
1012 http://www.itcmp.pwr.wroc.pl/~znmp/dydatyka/fundam_FM/Lecture_no3_Turbule

1013 nt_Flow_Modelling.pdf. Accessed on 15/04/2019

1014 Kumara, W.A.S., Halvorsen, B.M., Melaaen, M.C., 2010a. Single-beam gamma
1015 densitometry measurements of oil–water flow in horizontal and slightly inclined
1016 pipes. *Int. J. Multiph. Flow* 36, 467–480.

1017 Kumara, W.A.S., Halvorsen, B.M., Melaaen, M.C., 2010b. Single-beam gamma
1018 densitometry measurements of oil – water flow in horizontal and slightly inclined
1019 pipes. *Int. J. Multiph. Flow* 36, 467–480.
1020 <https://doi.org/10.1016/j.ijmultiphaseflow.2010.02.003>

1021 Kumara, W.A.S., Halvorsen, B.M., Melaaen, M.C., 2010c. Particle image velocimetry
1022 for characterizing the flow structure of oil – water flow in horizontal and slightly
1023 inclined pipes. *Chem. Eng. Sci.* 65, 4332–4349.
1024 <https://doi.org/10.1016/j.ces.2010.03.045>

1025 Kumara, W.A.S., Halvorsen, B.M., Melaaen, M.C., 2009. Pressure drop flow pattern
1026 and local water volume fraction measurements of oil-water flow in pipes. *Meas.*
1027 *Sci. Technol.* 1–25.

1028 Liu, W., Tan, C., Dong, F., 2021. Doppler spectrum analysis and flow pattern
1029 identification of oil-water two-phase flow using dual-modality sensor. *Flow Meas.*
1030 *Instrum.* 77, 101861. <https://doi.org/10.1016/j.flowmeasinst.2020.101861>

1031 Liu, Y., Deng, Y., Zhang, M., Yu, P., Li, Y., 2017. Experimental measurement of oil –
1032 water two-phase flow by data fusion of electrical tomography sensors and venturi
1033 tube. *Meas. Sci. Technol.* 28, 15.

1034 Lovick, J., Angeli, P., 2004. Experimental studies on the dual continuous flow pattern in
1035 oil – water flows. *Int. J. Multiph. Flow* 30, 139–157.
1036 <https://doi.org/10.1016/j.ijmultiphaseflow.2003.11.011>

1037 Lucas, G.P., Jin, N.D., 2001. Investigation of a drift velocity model for predicting
1038 superficial velocities of oil and water in inclined oil-in-water pipe flows. *Meas.*
1039 *Sci. Technol.* 12, 1546–1554.

1040 Mazza, R.A., Suguimoto, F.K., 2019. *Journal of Petroleum Science and Engineering*
1041 Experimental investigations of kerosene-water two-phase flow in vertical pipe. *J.*
1042 *Pet. Sci. Eng.* 106580. <https://doi.org/10.1016/j.petrol.2019.106580>

1043 Meribout, M., Al-Rawahi, N.Z., Al-Naamany, A.M., Al-Bimani, A., Al-Busaidi, K.,
1044 Meribout, A., 2010. A Multisensor intelligent device for real-time multiphase flow
1045 metering in oil fields. *Instrum. Meas. IEEE Trans.* 59, 1507–1519.

1046 Morriss, S.L., Hill, A.D., 1991. Measurement of velocity profiles in upwards oil/water
1047 flow using ultrasonic Doppler velocimetry, in: *SPE Annual Technical Conference*
1048 *and Exhibition*. Dallas, TX.

1049 Murai, Y., Tasaka, Y., Nambu, Y., Takeda, Y., A, S.R.G., 2010. Ultrasonic detection of
1050 moving interfaces in gas – liquid two-phase flow. *Flow Meas. Instrum.* 21, 356–
1051 366. <https://doi.org/10.1016/j.flowmeasinst.2010.03.007>

1052 Oddie, G.M., 1992. On the detection of a low-dimensional attractor in disperse two-
1053 component (oil-water) flow in a vertical pipe 2, 225–231.

1054 Onda, C., 2003. *Acoustic Properties of Liquids*.

1055 Paolinelli, L.D., 2020. A comprehensive model for stability of dispersed oil-water flow
1056 in horizontal and inclined pipes. *Chem. Eng. Sci.* 211, 115325.
1057 <https://doi.org/10.1016/j.ces.2019.115325>

1058 Picchi, D., Strazza, D., Demori, M., Ferrari, V., Poesio, P., 2015. An experimental
1059 investigation and two-fluid model validation for dilute viscous oil in water
1060 dispersed pipe flow. *Exp. Therm. Fluid Sci.* 60, 28–34.

- 1061 <https://doi.org/10.1016/j.expthermflusci.2014.07.016>
- 1062 Rodriguez, O.M.H., Oliemans, R.V.A., 2006. Experimental study on oil – water flow in
1063 horizontal and slightly inclined pipes. *Int. J. Multiph. Flow* 32, 323–343.
1064 <https://doi.org/10.1016/j.ijmultiphaseflow.2005.11.001>
- 1065 Rothfuss, M.A., Unadkat, J. V., Gimbel, M.L., Mickle, M.H., Sejdi, E.C., 2016. Totally
1066 implantable wireless ultrasonic Doppler blood flowmeters : toward accurate
1067 miniaturized chronic monitors. *Ultrasound Med. Biol.* 1–18.
1068 <https://doi.org/10.1016/j.ultrasmedbio.2016.11.005>
- 1069 Sanderson, M.L., Yeung, H., 2002. Guidelines for the use of ultrasonic non-invasive
1070 metering techniques. *Flow Meas. Instrum.* 13 13, 125–142.
- 1071 Shamsul, A., Ismail, Izwan, Ismail, Issham, Zoveidavianpoor, M., 2015. Review of oil –
1072 water through pipes. *Flow Meas. Instrum.* 45, 357–374.
1073 <https://doi.org/10.1016/j.flowmeasinst.2015.07.015>
- 1074 Shi, X., Dong, X., Tan, C., Dong, F., 2017. Velocity measurement of oil-water two-
1075 phase flow based on ultrasonic Doppler. *IEEE Trans. Instrum. Meas.*
- 1076 Stahl, P., von Rohr, P.R., 2004. On the accuracy of void fraction measurements by
1077 single-beam gamma-densitometry for gas–liquid two-phase flows in pipes. *Exp.*
1078 *Therm. Fluid Sci.* 28, 533–544.
- 1079 Tan, C., Dai, W., Yeung, H., Dong, F., 2015. A Kalman estimation based oil – water
1080 two-phase flow measurement with CRCC. *Int. J. Multiph. Flow* 72, 306–317.
1081 <https://doi.org/10.1016/j.ijmultiphaseflow.2014.06.014>
- 1082 Tan, C., Murai, Y., Liu, W., Tasaka, Y., Dong, F., Takeda, Y., 2021. Ultrasonic Doppler
1083 Technique for Application to Multiphase Flows : A Review. *Int. J. Multiph. Flow.*
1084 <https://doi.org/10.1016/j.ijmultiphaseflow.2021.103811>

- 1085 Tan, C., Yuan, Y., Dong, X., Dong, F., 2016. Oil-water two-phase flow measurement
 1086 with combined ultrasonic transducer and electrical sensors. Meas. Sci. Technol. 27.
 1087 <https://doi.org/10.1088/0957-0233/27/12/125307>
- 1088 Tesi, A.I.M., 2011. Multiphase flow measurement using gamma-based techniques, PhD
 1089 Thesis,. Cranfield University.
- 1090 Thorn, R., Johansen, G.A., Hjertaker, B.T., 2013. Three-phase flow measurement in the
 1091 petroleum industry. Meas. Sci. Technol. 24, 17. [https://doi.org/10.1088/0957-](https://doi.org/10.1088/0957-0233/24/1/012003)
 1092 [0233/24/1/012003](https://doi.org/10.1088/0957-0233/24/1/012003)
- 1093 Wallis, G.B., 1969. One Dimensional Two-Phase Flow. McGraw Hill Book Co. Inc.,
 1094 New York City.
- 1095 Yin, P., Cao, X., Zhang, P., Yang, W., Bian, J., Guo, D., 2019. Investigation of slug
 1096 flow characteristics in hilly terrain pipeline using ultrasonic Doppler method.
 1097 Chem. Eng. Sci. 115300. <https://doi.org/10.1016/j.ces.2019.115300>
- 1098 Zhai, L., Jin, N., Gao, Z., Wang, Z., Li, D., 2013. The ultrasonic measurement of high
 1099 water volume fraction in dispersed oil-in-water flows. Chem. Eng. Sci. 94, 271–
 1100 283. <https://doi.org/10.1016/j.ces.2013.02.049>

1101

1102 **7 Appendix**

1103 **7.1 Solution to equation (2-28)**

$$\bar{v}_{dop} = 2.5u_{\tau} \ln \frac{u_{\tau}\rho_m R}{\mu_m} + 1.75u_{\tau} \quad (\text{A-1})$$

$$\bar{v}_{dop} = Bu_{\tau} \ln Ku_{\tau} + Au_{\tau} \quad (\text{A-2})$$

1104 $B = 2.5, A = 1.75, K = \frac{\rho_m R}{\mu_m}$

1105 Equation (A-1) can be solved in similar expansion method as in Tan et al. (2016). The
 1106 expansion $\ln x = (x - 1) + \sum_{n=0}^{\infty} \frac{(-1)^n (x-1)^n}{n+1} \approx x - E$ was used to transform the
 1107 equation (A-2) as :

$$Bu_t^2 + (A + B \ln K - B * E)u_\tau - \bar{v}_{dop} = 0 \quad (A-3)$$

$$1108 \quad a = B$$

$$1109 \quad b = A + B \ln K - B * E$$

$$1110 \quad c = -\bar{v}_{dop}$$

1111 E is a compensation coefficient, which is dependednt on the nature of the flow. In this
 1112 study, most of the experiments are in dispersed flow and the value of $E = 3.3$ for a
 1113 dispersed flow (Tan et al., 2016).

1114 Solving the quadratic equation (A-3), the following expression for u_τ , the shear velocity
 1115 can be obtained:

$$u_\tau = \frac{-b + \sqrt{b^2 - 4ac}}{2a} \quad (A-4)$$

1116 Finally, the mixture velocity V_m can be calculated from the Eqn. (2-29)

1117 **8 Acknowledgements**

1118 We are grateful for the sponsorship from the Petroleum technology development fund
 1119 (PTDF, Nigeria) under the overseas scholarship scheme for PhD programme at
 1120 Cranfield University. Dr Baba Musa Abbagoni is particularly thankful to the PTDF for
 1121 sponsoring his postgraduate studies.

Nomenclature

\bar{f}_d average frequency shift reflected by the multiple droplets

E_r relative error of the estimation

ε_{ave}	average absolute of the error of the estimation
A_p	pipe cross-sectional area, m^2
C_o	flow distribution parameter,
I_0	Initial gamma intensity
U_{ow}	drift flux between the phases
V_{∞}	Terminal rise velocity
c_{ow}	sound speed in the oil/water mixture
f_m	two-phase friction factor
f_{max}	maximum Doppler frequency
f_t	transmitted frequency
k_m	mixture compressibility
u^+	dimensionless velocity
u_{τ}	shear velocity m/s
\bar{v}	Average velocity of droplets in the measuring volume
y^+	dimensionless wall distance
ρ_m	mixture density
D	flow pipe internal diameter, m
DP	differential pressure
E	compensation coefficient
I	received gamma intensity
$P(f)$	Doppler power spectrum
Q	volume flow rate (oil + water)
Re	Reynolds number, dimensionless

V	measured mean superficial flow velocity
V	measured mean superficial flow velocity
b	friction factor's coefficient
c	speed of the sound,
g	acceleration due to gravity
k	compressibility
m	Exponent of the drift velocity,
n	friction factor's exponent
$u(ow)$	flow velocity profile
z	distance gamma ray travelled through the absorbing medium

Greek letters

σ_{ow}	interracial tension,
φ_a	linear absorption coefficient in the air
φ_o	linear absorption coefficient for oil
φ_p	linear absorption coefficient in the pipe wall material
φ_w	linear absorption coefficient for water
z	distance travelled through the absorbing medium
Φ	is the angle of inclination of the flow pipe from the horizontal.
α	time-averaged local volume fraction
θ	angle between the ultrasonic beam and the pipe axis
μ	dynamic viscosity
ρ	flow density,
τ	wall shear stress,

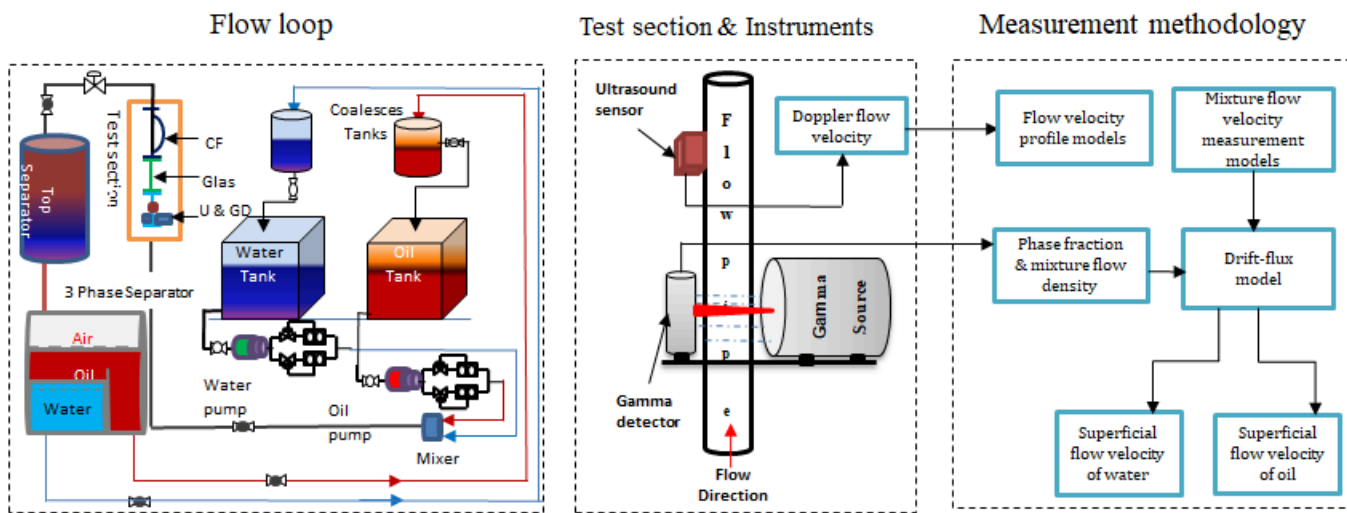
φ gamma absorption coefficient;

Subscripts

- m oil-water mixture
- o oil flow phase
- so superficial for oil phase
- sw superficial for water phase
- w water flow phase
- z distance travelled through the absorbing medium

Subscripts

- m oil-water mixture
- o oil flow phase
- so superficial for oil phase
- sw superficial for water phase
- w water flow phase



1122

1123 **Graphical abstract**

1124

1125 **Highlights**

- 1126 ▪ A method of measurement of of flow velocity in oil-water two-phase vertical
1127 flow using a non-invasive ultrasound Doppler sensor is developed
- 1128 ▪ We present flow velocity measurement correlations for both oil-continuous flow
1129 and water-continuous flow
- 1130 ▪ We formulated the drift-flux model for estimation of superficial velocity of oil
1131 and of water from the measured two-phase flow velocity.
- 1132 ▪ The estimated results using this proposed method are in good agreement with
1133 the reference flowmeters.
- 1134
- 1135

Non-invasive measurement of oil-water two-phase flow in vertical pipe using ultrasonic Doppler sensor and gamma ray densitometer

Abbagoni, Baba Musa

2021-10-28

Attribution-NonCommercial-NoDerivatives 4.0 International

Abbagoni BM, Yeung H, Lao L. (2022) Non-invasive measurement of oil-water two-phase flow in vertical pipe using ultrasonic Doppler sensor and gamma ray densitometer. *Chemical Engineering Science*, Volume 248, Part B, February 2022, Article number 117218

<https://doi.org/10.1016/j.ces.2021.117218>

Downloaded from CERES Research Repository, Cranfield University